# Iron Boosts Antitumor Type 1 T-cell Responses and Anti-PD1 Immunotherapy

Sarah Porte, Alexandra Audemard-Verger, Christian Wu, Aurélie Durand, Théo Level, Léa Giraud, Amélie Lombès, Mathieu Germain, Rémi Pierre, Benjamin Saintpierre, et al.

# Iron boosts anti-tumor type 1 T-cell responses and anti-PD1 immunotherapy

Sarah Porte[1], Alexandra Audemard-Verger[2,3*], Christian Wu[1*], Aurélie Durand[1*], Théo Level[1*], Léa Giraud[1*], Amélie Lombès[1*], Mathieu Germain[1*], Rémi Pierre[1], Benjamin Saintpierre[1], Mireille Lambert[1], Cédric Auffray[1], Carole Peyssonnaux[1], François Goldwasser[4], Sophie Vaulont[1], Marie-Clotilde Alves-Guerra[1], Renaud Dentin[1], Bruno Lucas[1**] and Bruno Martin[1**]

[1]Université Paris-Cité, Institut Cochin, Centre National de la Recherche Scientifique (CNRS) UMR8104, Institut National de la Santé et de la Recherche Médicale (INSERM) U1016, 75014 Paris, France.

[2] Department of Internal Medicine, CHU de Tours, France

[3] University of Tours, Tours, France.

[4]Department of Medical Oncology, Cochin Hospital, Paris Cancer Institute CARPEM, Université Paris Cité, APHP. Centre, 75014 Paris, France.

**Corresponding author:** Dr. Bruno Martin (bruno.martin@inserm.fr), Cochin Hospital, 75014 Paris, France. Phone: 33-1-40516589; Fax: 33-1-40516535

* Authors contributed equally to this paper

** Authors contributed equally to this paper

**Running title:** Iron boosts anti-tumor type 1 T-cell responses

**Keywords: T cells, iron, IFN-γ, Immunotherapy, Cancer**

**Funding information:** This work was supported by grants from the "Ligue contre le Cancer", the "Association pour la Recherche contre le Cancer" and the "Groupement des Entreprises Françaises dans la Lutte contre le Cancer".

**Authors' disclosures:** The authors declare no potential conflicts of interest.

## ABSTRACT

Cancers only develop if they escape immunosurveillance, and the success of cancer immunotherapies relies in most cases on their ability to restore effector T-cell functions, particularly IFN-γ production. Revolutionizing the treatment of many cancers, immunotherapies targeting immune checkpoints such as PD1 can increase survival and cure patients. Unfortunately, although immunotherapy has greatly improved the prognosis of patients, not all respond to anti-PD1 immunotherapy, making it crucial to identify alternative treatments that could be combined with current immunotherapies to improve their effectiveness. Here, we show that iron supplementation significantly boosts T-cell responses *in vivo* and *in vitro*. The boost was associated with a metabolic reprogramming of T cells in favor of lipid oxidation. We also found that the "adjuvant" effect of iron led to a marked slowdown of tumor-cell growth after tumor-cell line transplantation in mice. Specifically, our results suggest that iron supplementation promotes antitumor responses by increasing IFN-γ production by T cells. In addition, iron supplementation improved the efficacy of anti-PD1 cancer immunotherapy in mice. Finally, our study suggests that, in cancer patients, the quality and efficacy of the antitumor response following anti-PD1 immunotherapy may be modulated by plasma ferritin levels. In summary, our results suggest the benefits of iron supplementation on the reactivation of antitumor responses and support the relevance of a fruitful association between immunotherapy and iron supplementation.

**SYNOPSIS:** The authors show that iron supplementation reactivates antitumor T-cell responses and improves anti-PD1 efficacy in mice. Preliminary analysis of plasma ferritin levels in patients with cancer treated with anti-PD1, suggests iron may also modulate anti-PD1 responses in humans.

## INTRODUCTION

The ability of the immune system to respond to tumor antigens has led to the development of cancer immunotherapy in humans (1). Immune checkpoints are control points of the immune system, corresponding, among others, to the expression by T cells of inhibitory molecules that block their effector functions (2–5). Revolutionizing the treatment of many cancers, immunotherapies targeting immune checkpoints such as PD1 and its ligand PD-L1 have shown limited toxic effects (6–8) and clinical efficacy (9–18). One of the aims of immunotherapy is to restore T-cell effector functions (9,10) and, more precisely, their IFN-γ production capacities. Indeed, IFN-γ-producing, tumor-infiltrating T lymphocytes, such as type 1 T-helper (Th1) $CD4^+$ or cytotoxic (Tc1) $CD8^+$ T cells are among the most important cell types involved in immunosurveillance. Silencing of the genes encoding IFN-γ or the IFN-γ receptor, as well as neutralization of IFN-γ using suitable antibodies, abolishes the efficacy of cancer therapies in many preclinical models (11–13).

Unfortunately, only 20-30% of patients successfully respond to anti-PD1 immunotherapy. To overcome this shortcoming, current strategies propose to combine immunotherapy with more traditional treatments such as chemotherapy and radiotherapy. However, immunotherapy, radiotherapy and chemotherapy have deleterious side effects and these toxicities may be additive or even synergistic in the case of co-treatments (14). It is therefore crucial to identify alternative treatments that can be combined with immunotherapies to improve their effectiveness while avoiding or limiting the occurrence of side effects.

It has been shown that magnesium enhances $CD8^+$ T cell–mediated antitumor immunity and improves the efficacy of anti-PD1 immunotherapy (15). Iron could also represent an alternative therapeutic option to promote T-cell effector functions. Indeed, iron deprivation through the use of either iron-deficient diet or an *in vitro* iron chelation strategy, impairs both

the activation and proliferative capacity of peripheral T cells (16–18). In addition, the role of iron as a vaccine adjuvant in T cell–mediated adaptive immunity has been reported, notably through the use of iron oxyde nanoparticles that promote Th1 $CD4^+$ and Tc1 $CD8^+$ T-cell responses (19). Finally, iron can also promote the production of proinflammatory cytokines, including GM-CSF and IL-2, by T cells (20). In humans, the link between cancer development and iron deficiency has been highlighted by several epidemiological studies (21–23).

In light of these considerations, we investigated whether iron could modulate antitumor T-cell responses. We found that iron supplementation significantly boosted T-cell responses *in vivo* and *in vitro*. This "adjuvant" effect resulted in a strong slowing down of tumor-cell growth after transplantation in mice. We then (**i**) deciphered the mechanisms by which iron exerted its antitumor effect, (**ii**) examined whether iron supplementation could enhance the efficacy of anti-PD1 immunotherapy and finally (**iii**) conducted a retrospective analysis of a cohort of patients to determine whether there was a correlation between patient plasma iron levels and their capacity to mount an efficient antitumor response upon their first cure of anti-PD1 immunotherapy.

## MATERIALS AND METHODS

### Mice

Eight to twelve weeks old mice were used for experiments unless otherwise indicated. C57BL/6 mice were obtained from Janvier laboratories. C57BL/6 OTII mice were initially obtained from Dr. Emmanuel Donnadieu, Institut Cochin, Paris. C57BL/6 OTII mice were then crossed with C57BL/6 Foxp3-GFP mice to obtain C57BL/6 OTII Foxp3-GFP mice. C57BL/6 Foxp3-GFP mice were initially obtained from Dr. Bernard Malissen, Centre d'Immunologie de Marseille-Luminy, France. C57BL/6 Foxp3-GFP, C57BL/6 OTII Foxp3-GFP and C57BL/6 CD3$\varepsilon^{-/-}$ mice were maintained in our own animal facilities, under specific pathogen-free conditions. Experiments were carried out in accordance with the guidelines of the French Veterinary Department. All procedures performed were approved by the ethics committee for animal experimentation n°APAFIS #15886-2017120710342762 and #37826-2022040516328367 and validated by the "Ministère de l'Enseignement Supérieur de la Recherche et de l'Innovation". Sample sizes were chosen to assure reproducibility of the experiments and in accordance with the 3R rules of animal ethics regulation.

### Special mouse diets

Iron-enriched (20g/kg) and control diet (0,2g/kg) were purchased from SAFE under the respective references U8958 version 0223 and U8958 version 0177. Mice were fed with these diets for 3 weeks before tumor-cell transplantation and maintained with either control or iron-enriched diet throughout the experiments.

### Cell lines

MC38 (Murine Colon carcinoma cell line) and LLC (Lewis Lung Carcinoma) tumor cell lines were originally obtained in 2010 from ATCC and then maintained in our lab. Authentication has been performed by the supplier. All these cell lines have not been re-authenticated within

the past year. These cell lines were not tested for mycoplasma contamination. Tumor cell lines were cultured in DMEM Glutamax medium (Life Technologies) containing sodium pyruvate (1mM; Gibco), Hepes (0.01M; Gibco), non-essentials amino-acids (1X; Gibco), penicillin (50U/ml; Gibco), Streptomycin (50µg/ml; Gibco), β-mercapto-ethanol (0.034N; Sigma) and 10% FCS (Eurobio Scientific). After thawing, two passages maximum of the tumor cells were performed before use in the described experiments.

**Tumor transplantations**

C57BL/6 mice were fed with an iron enriched (iron 20g/kg) or control diet for 3 weeks (iron 0,2g/kg). C57BL/6-derived MC38 colon carcinoma or LLC lung carcinoma cells were washed three times in PBS and $10^6$ cells subcutaneously injected in the right flank of the mice under short-term inhalation anesthesia with isoflurane. Tumor sizes were measured using a caliper. Tumor surface areas were then calculated as tumor surface = length x width. Overall well-being was assessed every two days. Two to three weeks after tumor implantation, mice were sacrificed by cervical dislocation and tumors were isolated by surgical excision.

**Anti-PD1 immunotherapy in mice**

For anti-PD1 immunotherapy, tumor-bearing mice were intraperitoneally injected with 100µg of Ultra-LEAF anti-mouse PD-1 antibody (RMP1-14; Biolegend) every 3 days once tumor size reached 20-25$mm^2$, for a round of 5 injections.

**Patients**

The study was conducted in accordance with the ethical standards of the Helsinki Declaration and was approved by the Institutional Review Board. All patients gave written informed consent. We had access to a cohorte of 27 adult patients, 15 males and 12 females as reported in our manuscript. Findings apply to both sex male and female. Sex was determined based on self-reporting. Sex was considered in our data analysis as reported in the manuscript. We

performed a retrospective analysis of plasmas from cancer patients treated with immunotherapy (nivolumab; anti-PD1 immunotherapy) as per standard of care. More precisely, we analyzed plasmas from patients just before the first nivolumab cure (day 0) and after their first treatment with nivolumab immunotherapy (day 15). Only plasmas from patients with lung cancer were analyzed. Plasmas were collected between 2015 and 2016 and stored at -80°C in Cochin Hospital. The study was authorized by the local ethical committee of Cochin Hospital and Paris Cité University (CLEC 2023/185).

**Iron, ferritin and transferrin measurement**

Serum was collected from mice at the end of experimentation and iron status (iron, ferritin and transferrin) was measured by the biochemistry platform at the Center for Research on Inflammation (CRI; UMR 1149 INSERM) on an Olympus AU400 (Olympus and Beckman Coulter).

Plasma was collected from patients and iron status (iron, ferritin and transferrin) was measured by the biochemistry department of Cochin Hospital. Transferrin concentrations were measured on a cobas c701 analyzer (Roche Diagnostics Meylan) and ferritin concentrations were measured using the FERRI ECLIA assay on a cobas E801 analyzer (Roche Diagnostics Meylan). According to the manufacturer, the range of the assay extended from 0.5 to 2,000 µg/L. Samples containing ferritin >2,000 µg/L were automatically diluted 1:50. Iron concentrations were measured on a cobas c501 analyzer (Roche Diagnostics Meylan). Physicians in charge of the patients were blinded to the results of biomarkers, and biologists were blinded to the emergency diagnosis suspected by physicians.

**Cell suspensions**

Peripheral lymph nodes (pooled superficial cervical, axillary, brachial, inguinal, pLNs) and mesenteric lymph nodes (mLNs) were homogenized and passed through a nylon cell strainer (40µM; BD Falcon) in RPMI GlutaMAX (Life Technologies) supplemented with 10% FCS

(Eurobio scientific) for cell culture or in 5% FCS, 0.1% $NaN_3$ (Sigma-Aldrich) in PBS for flow cytometry. Tumors were minced and digested with Collagenase A (1mg/mL; Roche) and DNase I grade II (0,1 mg/mL; Roche) for 20min at 37°C, then homogenized in PBS, FCS 10% and passed through a nylon cell strainer (100μM; BD Falcon).

**Cell surface and intracellular staining and flow cytometry**

Cell suspensions were collected as described (see *Cell suspensions*) and dispensed into 96-well round-bottom microtiter plates (Greiner Bioscience; $6x10^6$ cells/well). Surface staining was performed as previously described (24). The antibodies used in the study are indicated in supplementary table S1. Briefly, cells were incubated on ice, for 15 min/step, with antibodies (Abs) in 5% FCS (Eurobio Scientific), 0.1% $NaN_3$ (Sigma-Aldrich) in PBS. Each cell staining reaction was preceded by a 15-min incubation with a purified anti-mouse CD16/32 Ab (FcgRII/III block; 2.4G2, BioXcell). The Foxp3 Staining Buffer Set (eBioscience) was used for Foxp3, Tbet, Gata3 and Rorγt intracellular staining. For determination of intracellular cytokine production, cells were stimulated with 0.5 μg/ml PMA (Sigma-Aldrich), 0.5 μg/ml ionomycin (Sigma-Aldrich), and 10 μg/ml BrefeldinA (Sigma-Aldrich) for 2 hrs at 37°C. Cells were then stained for surface markers, fixed in 2% paraformaldehyde in PBS, and permeabilized with 0.5% saponin, followed by labeling with cytokine-specific Abs.

Multi-color immunofluorescence was performed using a BD-Fortessa cytometer (BD Biosciences). List-mode data files were analyzed using Diva software V8 (BD Biosciences). Data acquisition and cell sorting were performed on the Cochin Immunobiology facility.

In this study, effector/memory $CD4^+$ T cells ($CD4_M$) were defined as $CD44^{hi}Foxp3^-CD4^+CD8\alpha^-TCR\beta^+$ cells and effector/memory $CD8^+$ T cells ($CD8_M$) as $CD44^{hi}Foxp3^-CD4^-CD8\alpha^+TCR\beta^+$ cells as defined by our gating strategy (Supplementary Fig. S1).

**List of used antibodies is shown in supplementary Table 1**

**Cell sorting**

$CD4^+$ and $CD8^+$ T cells were purified from LNs (pooled superficial cervical, axillary, brachial, inguinal, and mesenteric LNs) of C57BL/6 Foxp3-GFP mice by incubating cell suspensions on ice for 20 minutes with a mixture of anti-CD8 (53-6.7) or anti-CD4 (GK1.5), anti-CD11b (Mac-1), anti-Ter119 and anti-CD19 (1D3) Abs obtained from hybridoma supernatants, and then with magnetic beads coupled to anti-rat immunoglobulins (Dynal Biotech). Purified $CD4^+$ and $CD8^+$ T cells were then labeled with PE-Cy7-conjugated anti-CD44, PE-conjugated anti-CD25, anti-NK1.1, anti-TCRγ/δ, anti-CD11c, anti-CD11b, anti-CD19. The antibodies used are indicated in supplementary table S1. $CD4_N$ or $CD8_N$ T cells were flow cytometry sorted as $GFP^-Lin^-$ ($CD25^-NK1.1^-TCR\gamma/\delta^-CD11c^-CD11b^-CD19^-$) and $CD44^{-/lo}$ cells using a FACS-ARIA3 flow cytometer (BD Biosciences).

***In vitro* proliferation assay**

$CD4_N$ or $CD8_N$ T cells were labeled using a 5nM CellTrace violet (CTV) proliferation kit (Invitrogen) according to the manufacturer's guidelines. Cells were then cultured in RPMI Glutamax medium (Life Technologies) containing sodium pyruvate (1mM; Gibco), Hepes (0.01M; Gibco), non-essentials amino-acids (1X; Gibco), penicillin (50U/ml; Gibco), Streptomycin (50µg/ml; Gibco), β-mercapto-ethanol (0.034N; Sigma) and 10% FCS (Eurobio Scientific) at $2x10^5$ cells per well for 2 days in a 96-well plate coated with anti-CD3 (145-2C11, 4µg/mL) and anti-CD28 (37.51, 4µg/mL, Biolegend).

The average number of cell cycles was calculated as follows. First, we estimated the CTV dilution factor (*f*): CTV mean fluorescence intensity (MFI) of nondivided cells (cycle 0) divided by CTV MFI of the entire $CTV^+$ cell subset. Then, because the intracellular amount of CTV is halved during each cell cycle, the average number of cell cycles (*A*) was calculated using the following formula: $A = \log_2(f)$.

### *In vitro* Th1 polarization assays

Flow cytometry–sorted $CD4_N$ from LNs of C57BL/6 OTII Foxp3-GFP mice were stimulated for 4 days with either immobilized anti-CD3 (145-2C11, 4µg/mL, Biolegend) and anti-CD28 (37.51, 4µg/mL, Biolegend), or with splenocytes from C57BL/6 $CD3\varepsilon^{-/-}$ mice in presence of $OVA_{323-339}$ peptide (15µg/mL, Invivogen). In both assays, $CD4^+$ T cells were stimulated in the presence of graded concentrations of recombinant mouse IL-12 (R&D), of blocking anti-IL-4 (10 µg/mL, Biolegend) and in the presence or absence of Ferric Ammonium Citrate (FAC, 200µM).

### Cytokine multiplex assay

The levels cytokines in sera from mice and plasma from human were quantified by MSD multi-array V-PLEX assays (Meso Scale Discovery; Proinflammatory Panel 1 Mouse kit or Proinflammatory Panel 1 Human kit) according to the manufacturer's guidelines.

### RNA sequencing

Flow cytometry–sorted $CD4_N$ from LNs of C57BL/6 Foxp3-GFP mice (obtained as described above, see *Cell sorting*) were stimulated for 20 hours with anti-CD3 (145-2C11, 4µg/mL, Biolegend) and anti-CD28 (37.51, 4µg/mL, Biolegend) in the presence or absence of Ferric Ammonium Citrate (FAC, 200µM). After stimulation, $CD4^+$ T cells were once again flow-cytometry sorted to eliminate potential dead cells. Total RNA was extracted using an RNeasy Mini kit (QIAGEN). After RNA extraction, RNA concentrations were obtained using nanodrop or a fluorometric Qubit RNA assay (Life Technologies, Grand Island, New York, USA). The quality of the RNA (RNA integrity number) was determined on an Agilent 2100 Bioanalyzer (Agilent Technologies, Palo Alto, CA, USA) as per the manufacturer's instructions. To construct the libraries, 250 ng of high quality total RNA sample (RIN >9.1) was processed using Stranded mRNA Prep kit (Illumina) according to the manufacturer's

instructions. Briefly, after purification of poly-A–containing mRNA molecules, mRNA molecules were fragmented and reverse transcribed using random primers. Replacement of dTTP by dUTP during the second-strand synthesis achieved the strand specificity. Addition of a single A base to the cDNA was followed by ligation of Illumina adapters. Libraries were quantified by Q bit and profiles were assessed using the DNA High Sensitivity LabChip kit on an Agilent Bioanalyzer. Libraries were sequenced on an Illumina Nextseq 2000 instrument using 59 base-lengths read V2 chemistry in a paired-end mode.

After sequencing, a primary analysis based on AOZAN software (ENS, Paris) was applied to demultiplex and control the quality of the raw data (based of FastQC modules/version 0.11.5). Fastq files were then aligned using the STAR algorithm (version 2.7.6a) to the Ensembl release 109 Mus_musculus_GRCm39 reference.

Reads were then counted using RSEM (v1.3.1) and the statistical analyses on the read counts were performed with R (version 3.6.3) and the DESeq2 package (DESeq2_1.26.0) to determine the proportion of differentially expressed genes between two conditions.

We used the standard DESeq2 normalization method (DESeq2's median of ratios with the DESeq function), with a pre-filter of reads and genes (reads uniquely mapped on the genome, or up to 10 different loci with a count adjustment, and genes with at least 10 reads in at least 3 different samples). Following the package recommendations, we used the Wald test with the contrast function and the Benjamini-Hochberg FDR control procedure to identify the differentially expressed genes. R scripts and parameters are available on the platform, https://github.com/GENOM-IC-Cochin/RNA-Seq_analysis. The transcriptomic signatures of control and iron supplemented (FAC) activated $CD4^+$ T cells have been deposited in the Gene Expression Omnibus (NCBI) at http://www.ncbi.nlm.nih.gov/geo/ (accession number GSE262545)

**Mitochondrial stress test and glycolysis stress test**

Mitochondrial oxygen consumption (OCR) and extracellular acidification rate (ECAR) were measured in non-buffered medium using an XF96 extracellular flux analyzer (Seahorse, Agilent, CA, USA) as previously described (25,26). $8x10^5$ flow cytometry–sorted $CD4_N$ were cultured in Seahorse XF RPMI assay medium at pH 7.4, supplemented with 11 mM glucose and 2 mM glutamine (glucose stress test) or supplemented with 5 mM glucose, 150 mM BSA-conjugated palmitate and 2 mM glutamine (lipid stress test). All substrates were purchased from Seahorse, Agilent, CA, USA. After calibration of the analyzer, sequential compound injections, including oligomycin A (1 μM), carbonyl cyanide m-chlorophenyl hydrazone (CCCP; 6 μM), and finally antimycin (50 μg/mL) + rotenone (10 μM) were applied to test mitochondrial respiration. Etomoxir was used at 1 μM to inhibit lipid oxidation. Sequential compound injections, including glucose (11 mM), oligomycin A (1 μM), and 2-DG (50 mM), were applied to test glycolytic activity. OCR and ECAR values were normalized to cell number. All inhibitors were purchased from Sigma-Aldrich (Merck KGaA, Darmstadt, Germany).

**Generation of IFNγR1-KO MC38 tumor cells by Cas9/RNP nucleofection**

*Preparation of crRNA-tracrRNA duplex*

To prepare the duplex, each Alt-R crRNA and Alt-R tracrRNA (catalog number 1073189; IDT) was reconstituted to 100μM with Nuclease-Free Duplex Buffer (IDT). Oligos were mixed at equimolar concentrations in a sterile PCR tube (e.g., 1.5μl Alt-R crRNA and 1.5μl Alt-r tracrRNA). Oligos were annealed by heating at 95°C for 5min in PCR thermocycler and the mix was slowly cooled at room temperature.

*Precomplexing of Cas9/RNP*

In a PCR strip, two crRNA-tracrRNA duplexes (3µl equal to 150 pmol each, total 6µl) and 6µl (180 pmol) TrueCut Cas9 Protein v2 (catalog number A36499; Thermo Fisher Scientific) were gently mix by pipetting up and down and incubated at room temperature for at least 10 min. crRNA guides to target IFNγR1 were CTAGTCGCCAAGTCCGCAAG and GGTCCTGATGCTGTCTGCGA (designed by IDT).

*Nucleofection*

200µl complete tumor cell media (DMEM glutamax, Gibco + supplements) per well of a 96-well plate was prewarmed. $2x10^6$ tumor cells were resuspended in 20µl primary cell nucleofection solution (P3 Primary cell solution box; catalog number PBP3-00675; Lonza). Tumor cells were mixed and incubated in 12µl RNP in round bottom 96-well plate. The cell/RNP mix was transferred to Nucleofection cuvette strips (4D-Nucleofector X kit S; Lonza). Cells were electroporated using a 4D nucleofector (4D-Nucleofector Core Unit:Lonza, AAF-1002B; 4D-Nucleofector X Unit: AAF-1002X; Lonza). Pulses DN100 for tumor cells were used. After nucleofection, prewarmed tumor cell media was used to transfer transfected cells in $75cm^2$ culture flasks. Finally, knock-out clones were identified by traditional PCR using the primers CCGCCCCTGAAGAGCTGCCT and CAGAATCATCCTGCCAGCTG for IFNγR1.

**Statistics**

Data are expressed as mean ± SEM and the significance of differences between two series of results was assessed using Wilcoxon-Mann's Whitney U test unless otherwise indicated. Values of $p < 0,05$ were considered as statically significant (*$p < 0.05$; **$p < 0.01$; ***$p < 0.001$; ****$p < 0,0001$).

**Software for data collection and analysis**

Flow Cytometry: BD LSR and Fortessa (BD Biosciences), Cell Sorting: BD FACSAria III (BD Biosciences), DISCOVERY WORKBENCH (Meso Scale Discovery; MSD), Incucyte software (Sartorius). Flow Cytometry data were analyzed using DIVA 8.0.1 (BD Biosciences), Prism 8.2.1 (GraphPad) and Excel 15.29.1 (Microsoft). MSD data were analyzed using DISCOVERY WORKBENCH (Meso Scale Discovery; MSD) and Excel 15.29.1 (Microsoft).

**Data Availability Statement**

For RNA sequencing analysis, R scripts and parameters are available on the platform, https://github.com/GENOM-IC-Cochin/RNA-Seq_analysis. The data generated in this study concerning the transcriptomic signatures of control and iron supplemented (FAC) activated $CD4^+$ T cells have been deposited in the Gene Expression Omnibus (NCBI) at http://www.ncbi.nlm.nih.gov/geo/ (accession number GSE262545). All other data generated in this study are available within the article and its supplementary data files or from the corresponding author upon reasonable request.

## RESULTS

### Iron induces a strong slowdown of transplanted tumor growth in mice

MC38 or LLC tumor-cell lines were transplanted into C57BL/6 mice previously fed a control or iron-enriched diet (Fig. 1A, 1E). Growth of both tumor cell lines was significantly slowed in mice fed an iron-enriched diet (Fig. 1B, 1F). These results correlated with a lower tumor weight at sacrifice for mice fed an iron-enriched diet (Fig. 1B, 1F). As we expected, the serum iron level was greatly increased in mice fed an iron-enriched diet compared to those in the control group (Fig. 1C, 1G). Transferrin is the main iron transport protein in the organism. When iron stores are high, transferrin synthesis decreases as the body's iron needs are met. Ferritin is a protein responsible for body iron storage. In contrast to transferrin, ferritin levels increased in a proportional manner with the concentration of iron in the serum. Consistent with this, mice fed an iron-enriched diet had reduced serum transferrin levels while serum ferritin concentrations were greatly increased (Fig. 1C, 1G). In addition, serum transferrin saturation was strongly increased in these mice. The transferrin receptor CD71 is another classic marker whose expression is regulated by iron. We found that CD71 expression decreased on both memory $CD4^+$ and $CD8^+$ T cells recovered from the spleen of mice fed an iron-enriched diet compared to those in the control group (Supplementary Fig. S2A, S2B), confirming that these cells were effectively loaded with iron. This diminution was not associated with a reduction in the proliferative capacity of these cells, as illustrated by their KI67 expression (Supplementary Fig. S2C, S2D).

We observed that serum iron concentration and tumor weight at sacrifice were inversely correlated for both tumor-cell lines (Fig. 1D, 1H). Thus, we concluded that an iron-enriched environment strongly affects the growth of transplanted MC38 and LLC tumor cells.

**Iron impact on tumor growth mostly depends on T cells**

As iron may directly act on tumor-cell growth, we assessed whether iron could directly inhibit MC38 and LLC tumor-cell proliferation *in vitro*. As shown in Supplementary Fig. S3, the growth of both tumor-cell lines was not affected by increasing environmental iron levels, suggesting a critical role of the tumor microenvironment.

MC38 and LLC tumor-cell lines were then transplanted into T-cell deficient C57BL/6 CD3ε$^{-/-}$ mice fed a control or iron-enriched diet (Fig. 1I, 1K). In contrast to what we observed in T cell–competent mice, in T cell–deficient mice, tumor-cell growth and weight at sacrifice were not affected (LLC), or only slightly affected (MC38) by the iron-enriched diet (Fig. 1J, 1L). For the MC38 tumor-cell line, we therefore cannot exclude that other immune cell subsets, such as NK cells, may participate in the antitumor effects of iron. However, our results show that the iron-induced slowdown of tumor growth is mainly T-cell dependent.

**Iron supplementation increases the density of intratumoral type 1 effector T cells**

We then characterized the effector profile of tumor-infiltrating T lymphocytes (Fig. 2, Supplementary Fig. S4). In both tumor-cell transplantation models, the iron-enriched diet did not alter the proportions of regulatory Foxp3$^{+}$ CD4$^{+}$ T cells nor the proportions of effector/memory Th2 and Th17 cells, respectively characterized by the expression of the transcription factors GATA3 or RORγt and their capacity to produce IL-13 or IL-17 (Fig. 2A and Supplementary Fig. S4A). The proportions of CD4$^{+}$ Th1 and CD8$^{+}$ Tc1 cells, defined by the expression of the transcription factor Tbet and their capacity to produce IFN-γ, were increased in the MC38 tumor microenvironment in mice fed an iron-enriched diet compared to control group (Fig. 2A-2C). The proportion of effector CD4$^{+}$ T cells able to produce TNFα

within MC38 tumors isolated from mice fed an iron-enriched diet was also increased (Fig. 2A-2B). Moreover, higher densities of Tbet-expressing and IFN-γ-producing $CD4^+$ and $CD8^+$ T cells were observed in the MC38 tumor microenvironment of mice fed an iron-enriched diet (Fig. 2D). Finally, the proportions of Tbet-expressing cells among tumor-infiltrating $CD4^+$ and $CD8^+$ T cells were negatively correlated with tumor weight at sacrifice and positively correlated with mouse serum iron levels (Fig. 2E).

After LLC tumor-cell line transplantation, a similar increase in the proportions of $Tbet^+$ cells among tumor-infiltrating $CD4^+$ T cells was found in mice fed an iron-enriched diet (Supplementary Fig. S4A-S4B). The density of $Tbet^+$ $CD4^+$ T cells in the tumor microenvironment tended to be increased in mice fed an iron-enriched diet (Supplementary Fig. S3C). Once again, the proportions of Tbet-expressing $CD4^+$ T cells among tumor-infiltrating T cells were inversely correlated with the tumor weight at sacrifice and positively correlated with mouse serum iron levels (Supplementary Fig. S4D). Unlike the MC38 model, the proportions and densities of $CD8^+$ Tc1 cells were not increased in mice fed an iron-enriched diet (Supplementary Fig. S4B-S4C), and did not correlate with either the tumor weight or mouse serum iron levels (Supplementary Fig. S4D).

Thus, we conclude that increased iron levels in mice result in a greater density of intratumoral Th1 $CD4^+$ T cells and, in some cases, Tc1 $CD8^+$ T cells, and this correlates with a slowdown of tumor growth.

**Iron enhances T-cell activation and proliferation *in vitro***

Naive $CD4^+$ or $CD8^+$ T cells were stimulated in plates coated with anti-CD3 and anti-CD28 in the presence or absence of FAC. After stimulation, we observed, for both T-cell subsets, that the activation-induced increase in CD71 expression was significantly lower and very transient

in the presence of FAC (Supplementary Fig. S5) confirming that T cells in this setting were effectively iron loaded.

Changes in the expression of early activation markers such as loss of CD62L expression and acquisition of CD69 expression by T cells were then assessed (Fig. 3A-3B). Following stimulation, for both T-cell subsets, loss of CD62L expression as well as acquisition of CD69 expression occurred significantly more rapidly in the presence of FAC (Fig. 3A-3B). Consistent with this, the proliferation of both T-cell subsets was significantly enhanced in the presence of FAC (Fig. 3C-3D). Collectively, our data suggest that, *in vitro*, iron accelerates T-cell activation and increases T-cell proliferation rate.

**Iron induces T-cell metabolic reprogramming**

Glucose metabolism by T cells plays an important role during their activation (27). Metabolic requirements of T cells increase sharply upon activation, to support the biosynthesis of intracellular constituents such as lipid membranes, nucleic acids, and proteins. T cells can meet this demand by notably increasing glucose and glutamine metabolism. To assess whether iron supplementation could act on glucose metabolism to enhance the proliferation and activation rates of $CD4^+$ T cells, we performed a mitochondrial stress test assay using the Seahorse technology (11mM glucose and 2mM glutamine) (Supplementary Fig. S6A). FAC treatment reduced both basal and maximal respiration rate (OCR) of activated T cells. FAC treatment during glycolytic stress test (ECAR), also decreased both basal and maximal glycolytic capacities (Supplementary Fig. S6B). Thus, inhibition of glucose-dependent mitochondrial respiration was not compensated by enhanced glycolysis. Conversion of ECAR and OCR measurements into glycolytic and oxidative ATP production rates to assess the contribution of glycolysis and oxidative phosphorylation (OXPHOS) to overall $CD4^+$ T-cell

bioenergetics (28), revealed that glucose-dependent ATP production rate was significantly decreased in FAC treated activated $CD4^+$ T cells (Supplementary Fig. S6C).

To go further, we compared the transcriptome of naive $CD4^+$ T cells stimulated for 20 hours in plates coated with anti-CD3 and anti-CD28 in the presence (FAC) or absence (Ctrl.) of iron supplementation. With a fold change cut-off of $\geq 1.25$ and a *p*-value cut-off of $\leq 0.05$, we found that 226 genes were differentially expressed in $CD4^+$ T cells cultured in the presence of FAC when compared to their cell counterparts in the control group (61 genes were down-regulated; 165 genes were up-regulated) (Fig. 4A). Transcriptomic signature analysis, using QIAGEN Ingenuity Pathway Analysis, revealed that the seven most significant canonical pathways with the highest positive Z-score in $CD4^+$ T cells activated in the presence of FAC (numbered from the lowest p-value) were all related to lipid metabolism (Fig. 4B). Accordingly, the transcription of a large set of genes known to participate to lipid metabolism was up-regulated in $CD4^+$ T cells activated in the presence of FAC when compared to control group (Fig. 4C). Modulation of lipid oxidation in FAC-treated activated $CD4^+$ T cells could therefore boost their proliferation and activation. To test this hypothesis, we repeated our mitochondrial stress test using palmitate (150 mM) in combination with glucose (5 mM) and glutamine (2mM). In this setting, FAC treatment did not affect basal and maximal respiration rates or basal glycolytic activity of activated $CD4^+$ T cells (Supplementary Fig. S6D). However, inhibition of fatty acid oxidation using etomixir (a specific CPT1 inhibitor), only inhibited basal and maximal respiration rates or basal glycolytic activity of $CD4^+$ T cells activated in the presence of FAC (Fig. 4D-4E). Consistent with this, the rate of palmitate-dependent ATP production was significantly decreased in response to etomixir treatment (Fig. 4F). Moreover, this lipid dependency was specific to activated $CD4^+$ T cells, as etomoxir had no effect on unstimulated $CD4^+$ T cells (Supplementary Fig. S6E-S6F). These data overall

suggest that the increased activation of $CD4^+$ T cells when supplemented with iron is dependent on lipid oxidation.

**Iron promotes antitumor responses by enhancing T-cell IFN-γ production**

Our data suggest that increased iron levels in mice should result in a greater density of intra-tumoral IFN-γ-producing T cells. To assess whether iron supplementation can modulate the proportion of IFN-γ producing Th1 cells, at steady state, C57BL/6 mice were mated and fed either a control diet or an iron-enriched diet. The resulting litters were then maintained under control diet or an iron-enriched diet at weaning and analyzed at 10 weeks of age (Fig. 5A). The proportions of Tbet-expressing and IFN-γ-producing cells among memory $CD4^+$ T cells were increased in pLNs and spleen of iron-supplemented mice. However, our RNA-seq data did not suggest that iron promoted the differentiation of naive $CD4^+$ T cells towards the Th1 pathway upon activation as both "Th1" and "interferon gamma signaling" canonical pathways were turned off in $CD4^+$ T cells activated in the presence of FAC (Fig. 4B). Naïve $CD4^+$ T cells were then stimulated in plates coated with anti-CD3- and anti-CD28 and graded doses of IL-12 in the presence or absence of FAC (Fig. 5B-5C). In agreement with our RNA-seq analysis, we observed that iron supplementation did not increase the capacity of naïve $CD4^+$ T cells to produce IFN-γ and to differentiate into Th1 cells (Fig. 5B-5C). One possible hypothesis is that the observed "pro-Th1" boost effect of iron, might be indirect, through the "activation" of myeloid-cell populations (such as macrophages, dendritic cells or neutrophils) or lymphoid cells such as NK or B cells. To examine this hypothesis, we used an *in vitro* antigen-specific ($OVA_{323-339}$ peptide – OTII TCR transgenic CD4 $T_N$ cells) Th1 polarization assay. In this setting, iron supplementation strongly increased the capacity of naïve $CD4^+$ T

cells to produce IFN-γ and to differentiate into Th1 cells at high concentrations of IL-12 (Fig. 5D-5E), suggesting that the iron effect on Th1-cell generation might be indirect.

We then generated a MC38 tumor-cell line deficient for the expression of IFN-γ receptor 1 (MC38 IFN-γR1-KO) (Supplementary Fig. S7). In contrast to what we observed with control MC38 cells (Fig. 1), tumor growth and weight at sacrifice of MC38 IFN-γR1-KO tumor cells were unaffected or minimally affected by the iron-enriched diet (Fig. 5F-5G). However, proportions of IFN-γ-producing $CD4^+$ and $CD8^+$ T cells among tumor-infiltrating T lymphocytes were still increased in mice fed an iron-enriched diet (Fig. 5H). Altogether, our results suggest that the iron-enriched diet could exert its antitumor effect by boosting antitumor T-cell responses and in particular their capacity to produce IFN-γ.

**Iron boosts the effectiveness of anti-PD1 cancer immunotherapy**

As iron supplementation and anti-PD1 immunotherapy increase antitumor immune responses, causing tumor growth slowdown or arrest, we wondered if the effects of these two treatments administered at the same time could be additive or even synergistic (Fig. 6). MC38 tumor cells are known to be sensitive to anti-PD1 immunotherapy (29). Accordingly, MC38 tumor growth was affected by both treatments when given separately (Fig. 6A-6B). Interestingly, when iron supplementation and anti-PD1 immunotherapy were given in combination, tumor growth was even slower (Fig. 6B). Consistent with this, the survival of mice fed an iron-enriched diet and treated with an anti-PD1 was significantly longer than that of the other 3 experimental groups (Fig. 6C). While the median survival of mice that were subjected to iron supplementation or anti-PD1 immunotherapy was not significantly increased compared to the control group, the median survival of mice that received both treatments together was strongly and significantly augmented compared with all other groups (Fig. 6D). The extended survival

time, compared with the control group, revealed that the antitumor effect of the two combined treatments was significantly greater than the sum of the effects of the two treatments applied separately (Fig. 6E). Thus, when iron supplementation and anti-PD1 immunotherapy are combined, they may potentiate their anti-tumor effects. In agreement, we observed complete tumor regression in a large proportion of the mice (6 out of 15) that received the two treatments combined (Fig. 6E). In addition, PD-1 expression by memory $CD4^+$ or $CD8^+$ T cells was not modulated by iron, either in tumor dLNs or in the tumor (Supplementary Fig. S8A-S8B). In contrast, PD-L1 expression was significantly downregulated on tumor cells in mice fed an iron-enriched diet (Supplementary Fig. S8C-S8D), which is consistent with the fact that iron supplementation boosts the effectiveness of anti-PD1 cancer immunotherapy.

Unlike the MC38 tumor-cell line, LLC tumor cells are described as resistant to anti-PD1 immunotherapy (30). As we expected, tumor growth was delayed by iron supplementation, whereas anti-PD1 treatment, when given alone, had minimal effect (Fig. 6G-6H). However, when these two treatments were combined, tumor growth was much slower than that observed in the other groups (Fig. 6H). Accordingly, the survival of mice fed an iron-enriched diet and treated with anti-PD1 was significantly longer than that of mice that received a single treatment (Fig. 6I). Once again, the median survival of LLC tumor-cell transplanted mice that received both treatments was strongly and significantly increased compared to the 3 other groups (Fig. 6J). Finally, the extended survival time revealed that the antitumor effect of the two treatments combined was significantly greater than the sum of the effects of the two treatments applied separately (Fig. 6K), suggesting that iron supplementation and anti-PD1 immunotherapy may potentiate their impact on LLC tumor-cell development.

We also analyzed serum concentrations of antitumor T cell–associated cytokines such as IFN-γ, IL-2 and TNF-α from all groups. Mice transplanted with highly immunogenic MC38 tumor cells had elevated serum concentrations of IFN-γ, IL-2 and TNF-α, which were not

significantly increased by iron supplementation and/or anti-PD1 treatment (Supplementary Fig. S9). In contrast, we found that the serum levels of these cytokines were strongly increased in poorly immunogenic LLC tumor bearing mice fed an iron-enriched diet and treated with anti-PD1 (Supplementary Fig. S9).

Altogether, our data suggest that iron supplementation boosts the effectiveness of antiPD1 cancer immunotherapy, and may even render refractory tumor cells, such as LLC cells, sensitive to anti-PD1 immunotherapy.

**Body iron level modulates antitumor response quality and efficiency following anti-PD1 immunotherapy in cancer patients**

To investigate a potential relationship between plasma iron levels and the quality of antitumor response after anti-PD1 immunotherapy (nivolumab), we performed a retrospective analysis on 27 patients with lung cancer (Supplementary Table S2). We first analyzed the plasma ferritin levels of patients just before the first nivolumab dose (day 0; Fig. 7A). Among the 27 patients studied, 8 (~30%) had normal plasma ferritin levels while the remaining 19 (~70%) exhibited ferritin excess (plasma ferritin overload threshold: male>225μg/L; female>150μg/L) (Supplementary Table S2 and Fig. 7A). As previously mentioned, ferritin level increases proportionally to the concentration of iron in the plasma (Fig. 7B). However, ferritin is also an acute phase reactant protein and elevated ferritin is often related to acute or chronic inflammatory conditions. We observed that plasma levels of inflammatory markers such as CRP, albumin, orosomucoid and IgG were not significantly different between both patient groups at day 0 (Supplementary Table S2). Plasma ferritin might be therefore used as a surrogate marker of iron storage rather than inflammation in our patients. After the first treatment with nivolumab, patients with high plasma ferritin levels at day 0 had a significantly

higher probability of survival than patients with normal ferritin levels (Fig. 7C). While no differences could be detected for IL-6, IL-9, IL-10, IL-17A, IL-22, IL-33 or TARC (Supplementary Fig. S10) in the two groups of patients, we found that the plasma levels of Th1-related cytokines, i.e. IFN-γ, IFN-α, TNF-α, CXCL10 and CXCL11, which are associated with a good antitumor response, were increased 15 days after anti-PD1 treatment only in the plasma of patients with high ferritin levels at day 0 (Fig. 7D). Furthemore, IL-21 production, which has been described to have a potent antitumor effect (31–33), was also significantly increased only in patients with high plasma ferritin levels at day 0 (Fig. 7D).

Overall, our results suggest that the quality and efficacy of the antitumor response following anti-PD1 immunotherapy in cancer patients might be modulated by plasma iron levels.

## DISCUSSION

We have shown in this study that an iron-enriched environment strongly slows down tumor growth after transplantation of MC38 or LLC tumor cells in mice. The antitumoral iron effect is mainly T-cell dependent. Iron supplementation seems to improve antitumor immune responses by boosting T cells. Accordingly, we observed that iron supplementation enhanced *in vitro* T-cell activation and proliferation rates. Conversely, iron deprivation through an iron-deficient diet *in vivo* or iron chelation *in vitro* has been reported to impair both the activation and the proliferative capacity of peripheral T cells (16,17). It has been proposed that iron could contribute to activation-induced T-cell expansion by up-regulating IL-2R signaling and mitochondrial function (18). Our transcriptomic analyses suggest that iron supplementation also induces an important metabolic reprogramming in activated T cells. Indeed, iron supplementation may boost lipid biosynthesis in activated T cells, notably through the sterol regulatory element-binding protein (SREBP), a transcription factor controlling the expression of enzymes required for endogenous lipid synthesis, and the cholesterol biosynthesis pathways. Such a phenomenon has been described in primary human umbilical vein endothelial cells and in human atherosclerosis lesions, where iron retention in atherosclerosis plaque macrophages would contribute to cholesterol accumulation in these cells (34–36).

Instead of increasing glycolytic activity, we found that iron supplementation significantly and specifically increased lipid oxidation in activated $CD4^+$ T cells. Our results may seem contradictory to the main theory concerning the metabolic reprogramming required for efficient T-cell activation and proliferation. Indeed, to fulfill the energetic requirements associated with activation and rapid proliferation, it is commonly accepted that T cells modify their metabolic program to adopt aerobic glycolysis metabolism (37). However, a series of studies have revealed the importance of cellular fatty acid metabolism and the activation of

SREBP and cholesterol biosynthesis pathways for rapid T-cell proliferation (38–40). Indeed, in the absence of SREBP signaling, T cells are unable to blast, which results in attenuated clonal expansion during viral infection (38). Mechanistically, SREBP proteins are essential to meet the increased lipid requirements due to membrane synthesis during activation, blastogenesis and proliferation (38). In another study (40), it was shown that the mTOR-mediated signaling pathway is critical for SREBP-induced fatty acid biosynthesis and rapid proliferation of both murine and human $CD4^+$ T cells. The authors also highlighted that activated $CD4^+$ T cells use exogenous fatty acid as nutrients. Finally, it has been shown that linoleic acid potentiates the antitumor function of memory $CD8^+$ T cells by operating a profound metabolic reprogramming, conferring superior cytotoxic functions to these cells (41). Thus, by increasing lipid oxidation in activated T cells, iron supplementation could significantly enhance their activation and proliferation.

We also showed that tron supplementation leads to increased densities of intratumoral Tbet-expressing and IFN-γ producing pro-inflammatory type 1 effector T cells. Moreover, the fact that MC38 IFN-γR1-KO tumor cells were relatively unaffected by an iron-enriched diet after transplantation suggests that iron could exert its antitumor effect by boosting antitumor T-cell responses and in particular their capacity to produce IFN-γ. Th1 $CD4^+$ and Tc1 $CD8^+$ T cells are known to be among the most efficient effector-cell types involved in antitumor responses (11–13). The role of iron as a vaccine adjuvant to enhance adaptive immunity has been shown using iron oxyde nanoparticles that promote Th1 $CD4^+$ and Tc1 $CD8^+$ T-cell responses (19). In addition, iron accumulation can precipitate autoimmune disease such as experimental autoimmune encephalomyelitis by promoting pro-inflammatory cytokine production including IL-2, GMCSF, IFN-γ or TNF-α (20). However, our RNA-seq data suggest that unlike T-cell activation and proliferation, iron-induced metabolic reprogramming does not appear to be the underlying mechanism responsible for the increased capacity of naïve $CD4^+$

T cells to differentiate into Th1 cells. Our Th1 polarization assays suggest that the "pro-Th1" boost effect of iron that we observed *in vivo* might be indirect, through the "activation" of antigen-presenting cells (APCs) or lymphoid cells such as NK cells. Prior studies have shown that iron can modulate activation of APCs (42–47). Iron chelation leads to the down-regulation of MHC I molecule expression in macrophages (42). Conversely, iron oxide nanoparticles can significantly amplify type 1 interferon production leading to a more efficient maturation and activation of APCs (43). Other studies report that iron promotes the differentiation of macrophages toward the proinflammatory M1 phenotype (44–46) and can also favor NK-cell activation and their IFN-γ production (47). Iron may therefore indirectly promote the differentiation of naïve $CD4^+$ T cells toward the Th1 effector pathway.

In addition, we observed that iron supplementation boosts the effectiveness of anti-PD1 cancer immunotherapy, and can even render refractory tumor cells such as LLC cells sensitive to anti-PD1 immunotherapy. Moreover, iron and anti-PD1 treatments appear to potentiate their anti-tumor effects, even leading to complete tumor regression. We further observed that iron-boosted anti-PD1 immunotherapy was associated with increased mouse serum concentrations of IFN-γ, TNF-α and IL-2. Therapy combining monoclonal anti-PD1 and IL-2, during chronic LCMV infection, promotes the generation of highly functional effector LCMV-specific CD8 T cells (48). It can therefore be hypothesised that iron supplementation could also improve the efficacy of anti-PD1 cancer immunotherapy in mice by increasing IL-2 concentration levels, which may lead to the emergence of highly effective antitumor $CD8^+$ effector T cells.

In humans, a relationship between iron deficiency anemia and cancer development has been suggested by several epidemiological studies (49, 50). Anemia and cancer have often been linked due to the ability of cancer cells to sequester iron, thereby limiting iron availability for red blood–cell production (51, 52). Indeed, anemia is a feature of patients to varying degrees,

in virtually all types of cancer, and is often associated with a poor prognosis (51). For instance, 42.6% and 33% of patients with solid tumors or hematologic cancers respectively had iron deficiency and anemia (53). Iron deficiency anemia is also highly prevalent in colorectal cancer patients and may be associated with breast cancer progression (21–23). We found that after the first course of nivolumab, patients with high plasma ferritin levels had a significantly increased probability of survival compared with those without ferritin excess. After anti-PD1 treatment, the production of Th1-related cytokines, which are associated with a good antitumor response (54), was increased only in patients with high plasma ferritin levels, suggesting that, in cancer patients, the quality and efficiency of antitumor response following anti-PD1 immunotherapy may be modulated by the level of iron in the body. Individuals affected by iron-overload diseases such as hereditary hemochromatosis have a higher risk of developing hepatocellular carcinoma (55). The prognosis of hemochromatosis and most of its complications, including cancer development, is thought to be directly related to the extent, duration and chronicity of iron excess. However, in cancer patients, our data suggest that restoring normal iron levels prior to immunotherapy should have beneficial consequences by boosting antitumor responses without side effects. In summary, our data support the relevance of a fruitful association between immunotherapy and iron supplementation.

## AKNOWLEDGMENTS

We greatly acknowledge the Cochin Cytometry and Immunobiology (CYBIO), the Cochin genomic core facility (GENOM'IC), MOUSET'IC core facility and Cochin Animal Core facilities for their technological support. This work was supported by grants from the "Ligue contre le Cancer", the "Association pour la Recherche contre le Cancer" and the "Groupement des Entreprises Françaises dans la Lutte contre le Cancer".

## COMPETING INTERESTS

The authors declare that they have no competing interests.

## REFERENCES


1. Strebhardt K, Ullrich A. Paul Ehrlich's magic bullet concept: 100 years of progress. Nat Rev Cancer. 2008;8:473–80.

2. Nishimura H, Minato N, Nakano T, Honjo T. Immunological studies on PD-1 deficient mice: implication of PD-1 as a negative regulator for B cell responses. Int Immunol. 1998;10:1563–72.

3. Nishimura H, Nose M, Hiai H, Minato N, Honjo T. Development of lupus-like autoimmune diseases by disruption of the PD-1 gene encoding an ITIM motif-carrying immunoreceptor. Immunity. 1999;11:141–51.

4. Linsley PS, Ledbetter JA. The role of the CD28 receptor during T cell responses to antigen. Annu Rev Immunol. 1993;11:191–212.

5. Linsley PS, Clark EA, Ledbetter JA. T-cell antigen CD28 mediates adhesion with B cells by interacting with activation antigen B7/BB-1. Proc Natl Acad Sci U S A. 1990;87:5031–5.

6. Topalian SL, Hodi FS, Brahmer JR, Gettinger SN, Smith DC, McDermott DF, et al. Safety, activity, and immune correlates of anti-PD-1 antibody in cancer. N Engl J Med. 2012;366:2443–54.

7. Robert C, Long GV, Brady B, Dutriaux C, Maio M, Mortier L, et al. Nivolumab in previously untreated melanoma without BRAF mutation. N Engl J Med. 2015;372:320–30.

8. Borghaei H, Paz-Ares L, Horn L, Spigel DR, Steins M, Ready NE, et al. Nivolumab versus Docetaxel in Advanced Nonsquamous Non-Small-Cell Lung Cancer. N Engl J Med. 2015;373:1627–39.

9. Zitvogel L, Tesniere A, Kroemer G. Cancer despite immunosurveillance: immunoselection and immunosubversion. Nat Rev Immunol. 2006;6:715–27.

10. Waldman AD, Fritz JM, Lenardo MJ. A guide to cancer immunotherapy: from T cell basic science to clinical practice. Nat Rev Immunol. 2020;20:651–68.

11. Pitt JM, Vétizou M, Daillère R, Roberti MP, Yamazaki T, Routy B, et al. Resistance Mechanisms to Immune-Checkpoint Blockade in Cancer: Tumor-Intrinsic and -Extrinsic Factors. Immunity. 2016;44:1255–69.

12. Takeda K, Nakayama M, Hayakawa Y, Kojima Y, Ikeda H, Imai N, et al. IFN-γ is required for cytotoxic T cell-dependent cancer genome immunoediting. Nat Commun. 2017;8:14607.

13. Liu P, Zhao L, Pol J, Levesque S, Petrazzuolo A, Pfirschke C, et al. Crizotinib-induced immunogenic cell death in non-small cell lung cancer. Nat Commun. 2019;10:1486.

14. Yan Y, Kumar AB, Finnes H, Markovic SN, Park S, Dronca RS, et al. Combining Immune Checkpoint Inhibitors With Conventional Cancer Therapy. Front Immunol. 2018;9:1739.

15. Lötscher J, Martí I Líndez A-A, Kirchhammer N, Cribioli E, Giordano Attianese GMP, Trefny MP, et al. Magnesium sensing via LFA-1 regulates CD8+ T cell effector function. Cell. 2022;185:585-602.e29.

16. Bonaccorsi-Riani E, Danger R, Lozano JJ, Martinez-Picola M, Kodela E, Mas-Malavila R, et al.

Iron Deficiency Impairs Intra-Hepatic Lymphocyte Mediated Immune Response. PLoS One. 2015;10:e0136106.

17. Kuvibidila SR, Porretta C. Iron deficiency and in vitro iron chelation reduce the expression of cluster of differentiation molecule (CD)28 but not CD3 receptors on murine thymocytes and spleen cells. Br J Nutr. 2003;90:179–89.

18. Yarosz EL, Ye C, Kumar A, Black C, Choi E-K, Seo Y-A, et al. Cutting Edge: Activation-Induced Iron Flux Controls CD4 T Cell Proliferation by Promoting Proper IL-2R Signaling and Mitochondrial Function. J Immunol. 2020;204:1708–13.

19. Neto LMM, Zufelato N, de Sousa-Júnior AA, Trentini MM, da Costa AC, Bakuzis AF, et al. Specific T cell induction using iron oxide based nanoparticles as subunit vaccine adjuvant. Hum Vaccin Immunother. 2018;14:2786–801.

20. Wang Z, Yin W, Zhu L, Li J, Yao Y, Chen F, et al. Iron Drives T Helper Cell Pathogenicity by Promoting RNA-Binding Protein PCBP1-Mediated Proinflammatory Cytokine Production. Immunity. 2018;49:80-92.e7.

21. Rockey DC, Cello JP. Evaluation of the gastrointestinal tract in patients with iron-deficiency anemia. N Engl J Med. 1993;329:1691–5.

22. Ioannou GN, Rockey DC, Bryson CL, Weiss NS. Iron deficiency and gastrointestinal malignancy: a population-based cohort study. Am J Med. 2002;113:276–80.

23. Jian J, Yang Q, Dai J, Eckard J, Axelrod D, Axelrod D, et al. Effects of iron deficiency and iron overload on angiogenesis and oxidative stress-a potential dual role for iron in breast cancer. Free Radic Biol Med. 2011;50:841–7.

24. Delpoux A, Yakonowsky P, Durand A, Charvet C, Valente M, Pommier A, et al. TCR signaling events are required for maintaining CD4 regulatory T cell numbers and suppressive capacities in the periphery. J Immunol. 2014;193:5914–23.

25. Sancerni T, Renoult O, Luby A, Caradeuc C, Lenoir V, Croyal M, et al. UCP2 silencing restrains leukemia cell proliferation through glutamine metabolic remodeling. Front Immunol. 2022;13:960226.

26. Benichou E, Seffou B, Topçu S, Renoult O, Lenoir V, Planchais J, et al. The transcription factor ChREBP Orchestrates liver carcinogenesis by coordinating the PI3K/AKT signaling and cancer metabolism. Nat Commun. 2024;15:1879.

27. MacIver NJ, Michalek RD, Rathmell JC. Metabolic regulation of T lymphocytes. Annu Rev Immunol. 2013;31:259–83.

28. Mookerjee SA, Gerencser AA, Nicholls DG, Brand MD. Quantifying intracellular rates of glycolytic and oxidative ATP production and consumption using extracellular flux measurements. J Biol Chem. 2017;292:7189–207.

29. Ngiow SF, von Scheidt B, Akiba H, Yagita H, Teng MWL, Smyth MJ. Anti-TIM3 antibody promotes T cell IFN-γ-mediated antitumor immunity and suppresses established tumors. Cancer Res. 2011;71:3540–51.

30. Li HY, McSharry M, Bullock B, Nguyen TT, Kwak J, Poczobutt JM, et al. The Tumor Microenvironment Regulates Sensitivity of Murine Lung Tumors to PD-1/PD-L1 Antibody Blockade. Cancer Immunol Res. 2017;5:767–77.

31. Moroz A, Eppolito C, Li Q, Tao J, Clegg CH, Shrikant PA. IL-21 enhances and sustains CD8+ T cell responses to achieve durable tumor immunity: comparative evaluation of IL-2, IL-15, and IL-21. J Immunol. 2004;173:900–9.

32. Chapuis AG, Lee SM, Thompson JA, Roberts IM, Margolin KA, Bhatia S, et al. Combined IL-21-primed polyclonal CTL plus CTLA4 blockade controls refractory metastatic melanoma in a patient. J Exp Med. 2016;213:1133–9.

33. Shen S, Sckisel G, Sahoo A, Lalani A, Otter DD, Pearson J, et al. Engineered IL-21 Cytokine Muteins Fused to Anti-PD-1 Antibodies Can Improve CD8+ T Cell Function and Anti-tumor Immunity. Front Immunol. 2020;11:832.

34. Fisher AL, Srole DN, Palaskas NJ, Meriwether D, Reddy ST, Ganz T, et al. Iron loading induces cholesterol synthesis and sensitizes endothelial cells to TNFα-mediated apoptosis. J Biol Chem. 2021;297:101156.

35. Stadler N, Lindner RA, Davies MJ. Direct detection and quantification of transition metal ions in human atherosclerotic plaques: evidence for the presence of elevated levels of iron and copper. Arterioscler Thromb Vasc Biol. 2004;24:949–54.

36. Xiao L, Luo G, Guo X, Jiang C, Zeng H, Zhou F, et al. Macrophage iron retention aggravates atherosclerosis: Evidence for the role of autocrine formation of hepcidin in plaque macrophages. Biochim Biophys Acta Mol Cell Biol Lipids. 2020;1865:158531.

37. Pearce EL, Pearce EJ. Metabolic pathways in immune cell activation and quiescence. Immunity. 2013;38:633–43.

38. Kidani Y, Elsaesser H, Hock MB, Vergnes L, Williams KJ, Argus JP, et al. Sterol regulatory element-binding proteins are essential for the metabolic programming of effector T cells and adaptive immunity. Nat Immunol. 2013;14:489–99.

39. Muroski ME, Miska J, Chang AL, Zhang P, Rashidi A, Moore H, et al. Fatty Acid Uptake in T Cell Subsets Using a Quantum Dot Fatty Acid Conjugate. Sci Rep. 2017;7:5790.

40. Angela M, Endo Y, Asou HK, Yamamoto T, Tumes DJ, Tokuyama H, et al. Fatty acid metabolic reprogramming via mTOR-mediated inductions of PPARγ directs early activation of T cells. Nat Commun. 2016;7:13683.

41. Nava Lauson CB, Tiberti S, Corsetto PA, Conte F, Tyagi P, Machwirth M, et al. Linoleic acid potentiates CD8+ T cell metabolic fitness and antitumor immunity. Cell Metab. 2023;35:633-650.e9.

42. Sottile R, Federico G, Garofalo C, Tallerico R, Faniello MC, Quaresima B, et al. Iron and Ferritin Modulate MHC Class I Expression and NK Cell Recognition. Front Immunol. 2019;10:224.

43. Chen F, Li T, Zhang H, Saeed M, Liu X, Huang L, et al. Acid-Ionizable Iron Nanoadjuvant Augments STING Activation for Personalized Vaccination Immunotherapy of Cancer. Adv Mater. 2023;35:e2209910.

44. Cairo G, Recalcati S, Mantovani A, Locati M. Iron trafficking and metabolism in macrophages: contribution to the polarized phenotype. Trends Immunol. 2011;32:241–7.

45. Kroner A, Greenhalgh AD, Zarruk JG, Passos Dos Santos R, Gaestel M, David S. TNF and increased intracellular iron alter macrophage polarization to a detrimental M1 phenotype in the injured spinal cord. Neuron. 2014;83:1098–116.

46. Ni S, Yuan Y, Kuang Y, Li X. Iron Metabolism and Immune Regulation. Front Immunol. 2022;13:816282.

47. Littwitz-Salomon E, Moreira D, Frost JN, Choi C, Liou KT, Ahern DK, et al. Metabolic requirements of NK cells during the acute response against retroviral infection. Nat Commun. 2021;12:5376.

48. Hashimoto M, Araki K, Cardenas MA, Li P, Jadhav RR, Kissick HT, et al. PD-1 combination therapy with IL-2 modifies CD8+ T cell exhaustion program. Nature. 2022;610:173–81.

49. Beale AL, Penney MD, Allison MC. The prevalence of iron deficiency among patients presenting with colorectal cancer. Colorectal Dis. 2005;7:398–402.

50. Kuvibidila SR, Gauthier T, Rayford W. Serum ferritin levels and transferrin saturation in men with prostate cancer. J Natl Med Assoc. 2004;96:641–9.

51. Naoum FA. Iron deficiency in cancer patients. Rev Bras Hematol Hemoter. 2016;38:325–30.

52. Jung M, Mertens C, Tomat E, Brüne B. Iron as a Central Player and Promising Target in Cancer Progression. Int J Mol Sci. 2019;20:E273.

53. Ludwig H, Müldür E, Endler G, Hübl W. Prevalence of iron deficiency across different tumors and its association with poor performance status, disease status and anemia. Ann Oncol. 2013;24:1886–92.

54. Chraa D, Naim A, Olive D, Badou A. T lymphocyte subsets in cancer immunity: Friends or foes. J Leukoc Biol. 2019;105:243–55.

55. Kowdley KV. Iron, hemochromatosis, and hepatocellular carcinoma. Gastroenterology. 2004;127:S79-86.

## FIGURE LEGENDS

**Figure 1: Iron supplementation strongly slows the growth of transplanted MC38 and LLC tumor cells in mice in a T cell–dependent manner**

MC38 (A-D) or LLC (E-H) tumor cells were transplanted into C57BL/6 mice previously fed with either a control or an iron-enriched diet. (A, E) Experimental models. (B) MC38 tumor growth over time and tumor weight at the time of sacrifice. (C) Serum iron, transferrin and ferritin levels and serum transferrin saturation of MC38 tumor bearing mice at the time of sacrifice. (D) Correlation between serum iron level and MC38 tumor weight at the time of sacrifice. (F) LLC tumor growth over time and tumor weight at the time of sacrifice. (G) Serum iron, transferrin and ferritin levels and serum transferrin saturation of LLC tumor bearing mice at the time of sacrifice. (H) Correlation between serum iron level and LLC tumor weight at the time of sacrifice. MC38 (I-J) or LLC (K-L) tumor cells were transplanted into C57BL/6 CD3$\varepsilon^{-/-}$ mice fed with either a control or an iron-enriched diet. (I, K) Experimental models. (J) MC38 tumor growth over time and tumor weight at the time of sacrifice. (L) LLC tumor growth over time and tumor weight at the time of sacrifice. For assessing correlations, Pearson correlation (two-sided test, coefficient, and 95% confidence intervals) was used. Data are expressed as mean ± SEM for at least two independent experiments. Wilcoxon-Mann's Whitney test was used (*$p < 0.05$; **$p < 0.01$; ***$p < 0.001$; ****$p <$ 0,0001, ns, not significant.). Each dot on figure panels represents individual mice.

**Figure 2: Iron supplementation increases the density of type 1 effector T cells in the MC38 tumor microenvironment**

MC38 tumor cells were transplanted into C57BL/6 mice fed with either a control or an iron-enriched diet. (A) Radar plots illustrating the proportions of the different CD4 and CD8 T-cell subsets among tumor infiltrating T cells. (B) Representative IFN-γ, TNF-α and Tbet dotplots for gated tumor infiltrating memory CD4 and CD8 T cells. (C) Proportions of Tbet-expressing and IFN-γ-producing CD4 or CD8 T cells among tumor infiltrating memory $CD4_M$ or $CD8_M$ T cells. (D) Densities of $CD4_M$, $CD8_M$, Tbet-expressing and IFN-γ producing $CD4_M$ and $CD8_M$ T cells within tumor microenvironments. (E) Correlations between either MC38 tumor weight at the time of sacrifice or serum iron level with proportions of Tbet-expressing CD4 and CD8 T cells among tumor-infiltrating T cells. For assessing correlations, Pearson correlation (two-sided test, coefficient, and 95% confidence intervals) was used. Data are expressed as mean ± SEM (n = 3 independent experiments). Wilcoxon-Mann's Whitney test was used. (*$p < 0.05$; **$p < 0.01$; ***$p < 0.001$; ****$p <$ 0,0001, ns, not significant.). Each dot on figure panels represents individual mice.

**Figure 3: Iron increases T-cell activation and proliferation *in vitro***

(A, B) Naïve CD4 or CD8 T cells were stimulated for the indicated times with coated anti-CD3 and anti-CD28 antibodies in the presence or absence of FAC. (A) Representative CD62L and CD69 fluorescence histograms of CD4 or CD8 T cells, *ex vivo* or at different time after stimulation. (B) Proportions of $CD62L^-$ CD4 or CD8 T cells and $CD69^+$ CD4 or CD8 T cells 2h30 after the onset of culture. (C, D) Naïve CD4 or CD8 T cells were labeled with Cell Trace Violet (CTV) and cultured for 2 and 3 days with or without coated anti-CD3 and anti-CD28 Abs in the presence or absence of FAC. (C) Representative CTV fluorescence histograms of cultured CD4 or CD8 T cells. (D) Average number of cell cycles of CD4 or CD8 T cells 2 and 3 days after the onset of culture in the presence or absence of FAC. Data are expressed as mean ± SEM. Results were assessed using a two-tailed paired Student's *t*-test (**p* < 0.05; ***p* < 0.01; ****p* < 0.001; *****p* < 0,0001, ns, not significant.). Each dot on figure panels represents individual experiments.

**Figure 4: Iron induces T-cell metabolic reprogramming**

(A-C) RNA-seq analysis of naive CD4 T cells stimulated for 20 hours with coated anti-CD3 and anti-CD28 antibodies in the presence (FAC) or absence (Ctrl.) of iron supplementation. (A) Volcano plot showing the differentially expressed genes (fold change cut-off of ≥ 1.25 and a *p*-value cut-off of ≤0.05) between FAC-activated CD4 T cells and Ctrl. group. (B) p-value/Z score dot-plots representing the canonical pathways determined by Ingenuity Pathway Analysis software as significantly ($p < 0.05$) involved in the transcriptomic signature of FAC-activated CD4 T cells. (C) Heatmap of selected differentially expressed genes. (D-F) Oxidative and glycolytic capacities were determined using Seahorse in activated CD4 T cells treated or not with etomoxir in the presence (FAC) or absence (Ctrl.) of iron supplementation and incubated in the presence of palmitate/BSA, glucose and glutamine. (D) Basal and maximal respiration rate (OCR), and basal glycolytic capacity (ECAR) (n = 3 independent experiments). (E) Representative profile after mitochondrial stress assay showing the OCR of activated CD4 T cells treated with etomoxir, in the absence or presence of FAC (n = 3 independent experiments). (F) ATP production rate from glycolysis or oxidative phosphorylation in activated CD4 T cells treated or not with etomoxir in the presence of FAC. (n = 3 independent experiments). Data are expressed as mean ± SEM. Results were assessed using a two-tailed paired Student's *t*-test (**p* < 0.05; ***p* < 0.01; ****p* < 0.001; *****p* < 0,0001, ns, not significant.).

**Figure 5: Iron promotes antitumor responses by enhancing T-cell IFN-γ production**

(A) C57/BL6 mice were mated and fed either a control diet or an iron-enriched diet. The resulting litters were then maintained under control diet or an iron-enriched diet at weaning and analyzed at 10 weeks of age. Proportions of Tbet-expressing and IFN-γ-producing CD4 T cells among $CD4_M$ T cells recovered from litter peripheral LNs (pLNs), mesenteric LNs (mLNs) and spleen (n = 3 independent experiments; Wilcoxon-Mann's Whitney test was

used). (B-E) Facs sorted naïve CD4 T cells from C57BL/6 OTII mice were stimulated for 4 days in the presence of graded concentrations of IL-12, in the presence or absence of FAC with anti-CD3- and anti-CD28-coated antibodies (B, C) or with antigen presenting cells (total splenocytes from T-cell deficient mice) and $OVApep_{323-339}$ (D, E). Representative IFN-γ dot-plots for gated CD4 T cells (B, D) and the proportion of IFN-γ-producing CD4 T cells (C, E) are shown as a function of IL-12 concentration (n = 5 independent experiments; results were assessed using a two-tailed paired Student's *t*-test). MC38 IFN-γR1-KO or MC38 tumor cells were transplanted into C57BL/6 mice fed with either a control or an iron-enriched diet. (F) Experimental model. (G) MC38 IFN-γR1-KO and MC38 tumor growth over time and MC38 IFN-γR1-KO tumor weight at the time of sacrifice. (H) Proportions of Tbet-expressing and IFN-γ-producing CD4 or CD8 T cells among MC38 IFN-γR1-KO tumor infiltrating $CD4_M$ or $CD8_M$ T cells (n = 3 independent experiments; Wilcoxon-Mann's Whitney test was used). Data are expressed as mean ± SEM (*$p < 0.05$; **$p < 0.01$; ***$p < 0.001$; ****$p <$ 0,0001, ns, not significant.). Each dot on figure panels represents individual mice.

**Figure 6: Iron boosts the efficacy of anti-PD1 cancer immunotherapy in MC38 and LLC tumor-cell transplanted mice**

MC38 (A-E) or LLC (F-I) tumor cells were transplanted into C57BL/6 mice fed with either a control or an iron-enriched diet. For concerned groups, anti-PD1 immunotherapy was administered once tumor size reached 20-25$mm^2$. (A, G) Experimental models. (B) MC38 tumor growth over time for the different groups of mice. Statistics were calculated using 2way ANOVA analysis. Each curve represents individual mice. (n = 3 independent experiments) (C) Survival percentage over time for the different groups of mice transplanted with MC38 tumor cells. Significances were calculated using Log-Rank test. (D) Median survival for the different groups of mice transplanted with MC38 tumor cells. Statistics were calculated using one way ANOVA analysis. (E) Extended survival time, compared to control group, of MC38 tumor bearing mice that received the two treatments (iron diet + anti-PD1) either together or separately (iron diet or anti-PD1). In this latter case the sum of both has been calculated (Student's *t*-test). (F) Percentage of full tumor regression observed for anti-PD-1 treated mice. (H) LLC tumor growth over time for the different groups of mice. Statistics were calculated using 2way ANOVA analysis. Each curve represents individual mice. (n = 3 independent experiments) (I) Survival percentages over time for the different groups of mice transplanted with LLC tumor cells. Statistics were calculated using Log-Rank test. (J) Median survival for the different groups of mice transplanted with LLC tumor cells. Statistics were calculated using one way ANOVA analysis. (K) Extended survival time, compared to control group, of LLC tumor bearing mice that received the two treatments either together (iron diet + anti-PD1) or separately (iron diet or anti-PD1). In this latter case the sum of both has been calculated (Student's *t*-test). *$p < 0.05$; **$p < 0.01$; ***$p < 0.001$; ****$p <$ 0,0001, ns, not significant.

**Figure 7: Body ferritin level modulates the quality and efficacy of anti-tumor response after anti-PD1 immunotherapy in cancer patients**

(A) Ferritin concentration in plasma from male and female cancer patients before the first nivolumab cure (day 0). (B) Ferritin concentration in plasma from patients with normal or low iron level in plasma at day 0. Wilcoxon-Mann's Whitney test was used. (C) Cumulative survival probability over time following anti-PD1 immunotherapy of patients with normal plasmatic ferritin level versus patients with high plasmatic ferritin level at day 0. Kaplan-Meier test was used. (D) Plasma concentrations of indicated cytokine at day 0 and day 15 (after nivolumab cure) from patients with high or normal plasma ferritin level at day 0. Each dot represents individual patients. Data are expressed as median, Wilcoxon-Mann's Whitney test was used. (*$p < 0.05$; **$p < 0.01$; ***$p < 0.001$; ****$p <$ 0,0001, ns, not significant).

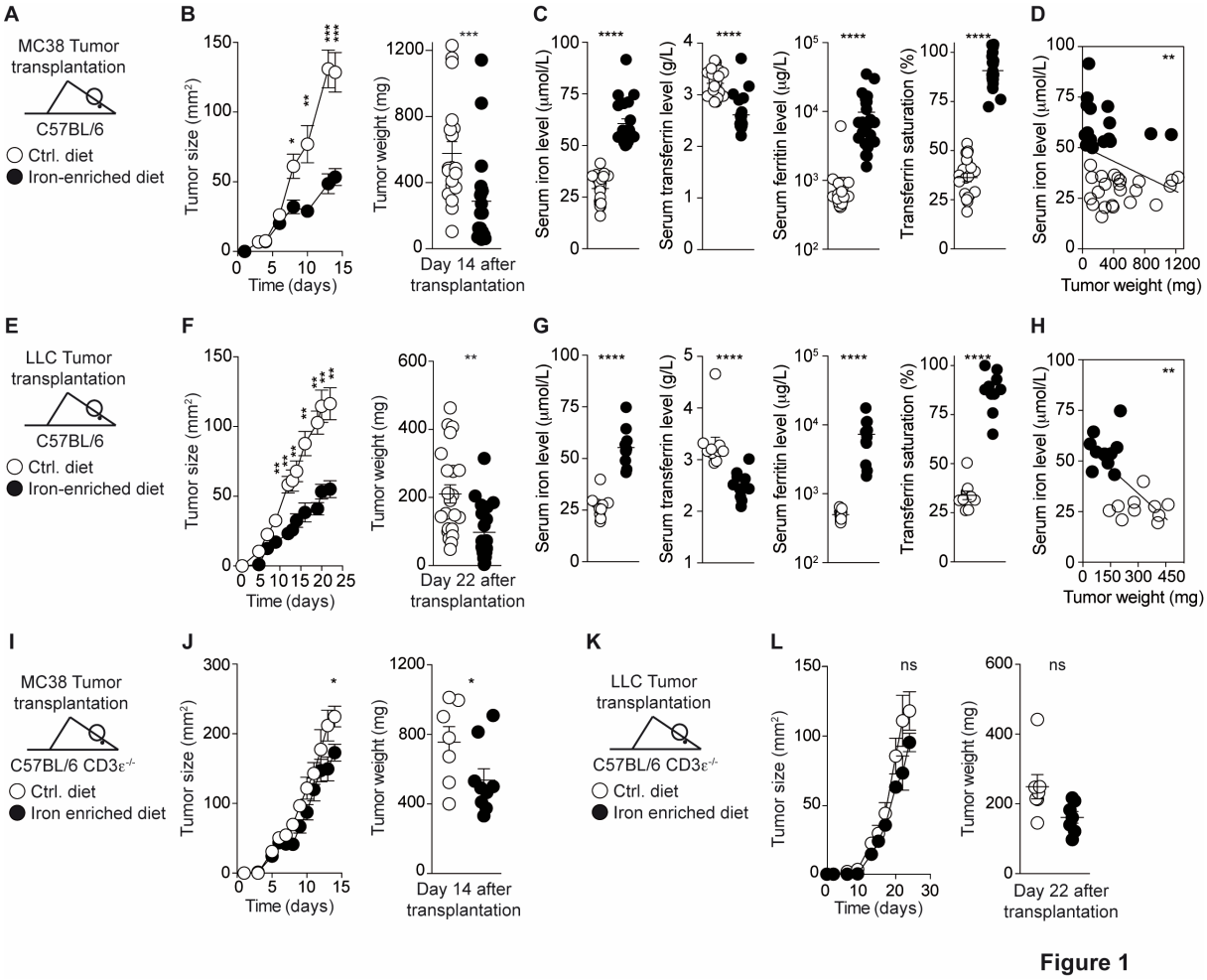
A
MC38 Tumor transplantation
C57BL/6
Ctrl. diet
Iron-enriched diet
B
Tumor size (mm²)
Time (days)
Tumor weight (mg)
Day 14 after transplantation
C
Serum iron level (µmol/L)
Serum transferrin level (g/L)
Serum ferritin level (µg/L)
Transferrin saturation (%)
D
Serum iron level (µmol/L)
Tumor weight (mg)
E
LLC Tumor transplantation
C57BL/6
Ctrl. diet
Iron-enriched diet
F
Tumor size (mm²)
Time (days)
Tumor weight (mg)
Day 22 after transplantation
G
Serum iron level (µmol/L)
Serum transferrin level (g/L)
Serum ferritin level (µg/L)
Transferrin saturation (%)
H
Serum iron level (µmol/L)
Tumor weight (mg)
I
MC38 Tumor transplantation
C57BL/6 CD3ε-/-
Ctrl. diet
Iron enriched diet
J
Tumor size (mm²)
Time (days)
Tumor weight (mg)
Day 14 after transplantation
K
LLC Tumor transplantation
C57BL/6 CD3ε-/-
Ctrl. diet
Iron enriched diet
L
ns
Tumor size (mm²)
Time (days)
Tumor weight (mg)
ns
Day 22 after transplantation

**Figure 1**

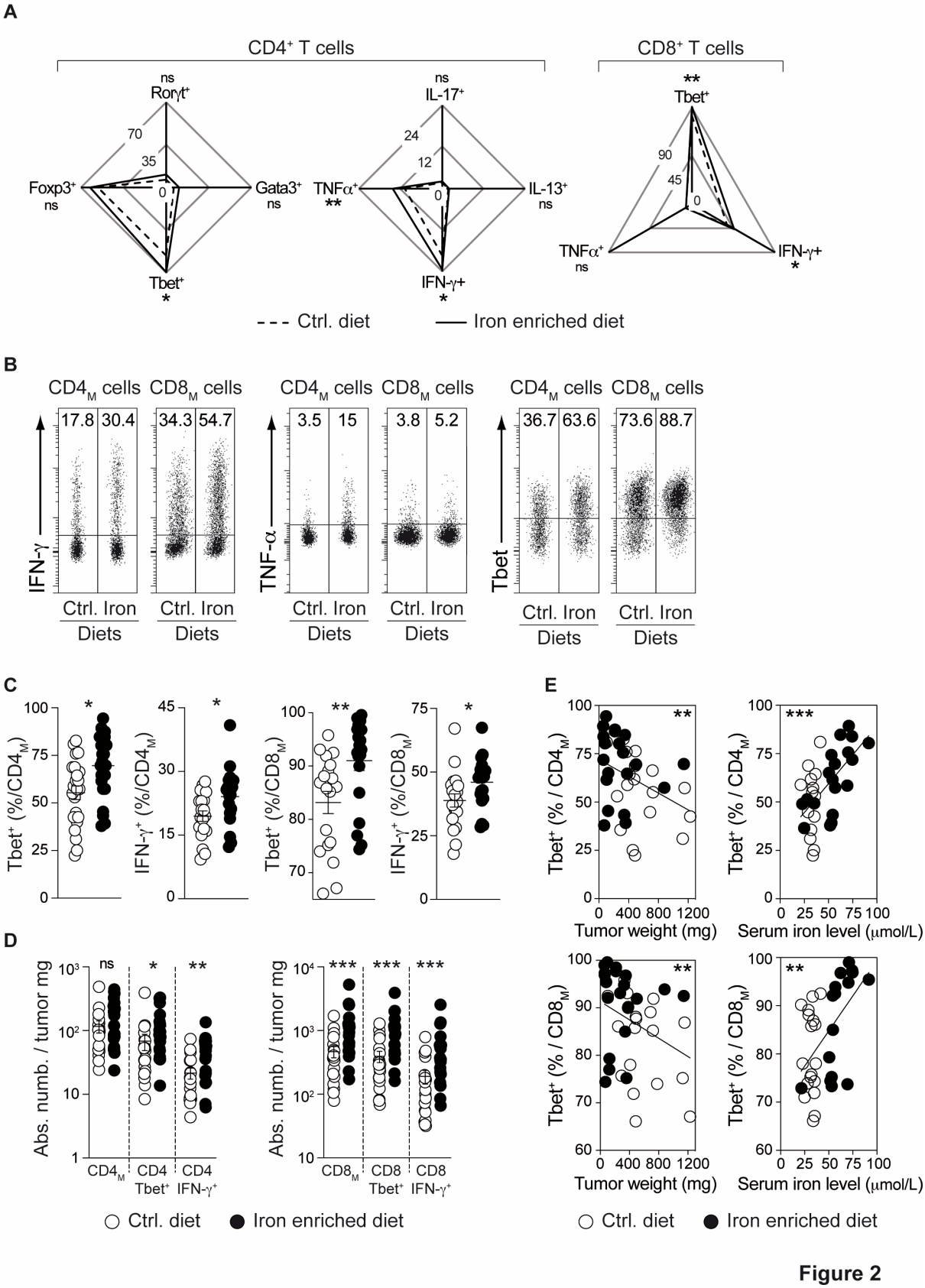
A
CD4+ T cells
CD8+ T cells
Rorγt+
IL-17+
Tbet+
Foxp3+
Gata3+
TNFα+
IL-13+
IFN-γ+
TNFα+
IFN-γ+
Ctrl. diet
Iron enriched diet
B
CD4M cells
CD8M cells
IFN-γ
TNF-α
Tbet
Ctrl. Iron
Diets
C
Tbet+ (%/CD4M)
IFN-γ+ (%/CD4M)
Tbet+ (%/CD8M)
IFN-γ+ (%/CD8M)
D
Abs. numb. / tumor mg
CD4M
CD4 Tbet+
CD4 IFN-γ+
CD8M
CD8 Tbet+
CD8 IFN-γ+
Ctrl. diet
Iron enriched diet
E
Tbet+ (% / CD4M)
Tbet+ (% / CD8M)
Tumor weight (mg)
Serum iron level (μmol/L)
Ctrl. diet
Iron enriched diet

**Figure 2**

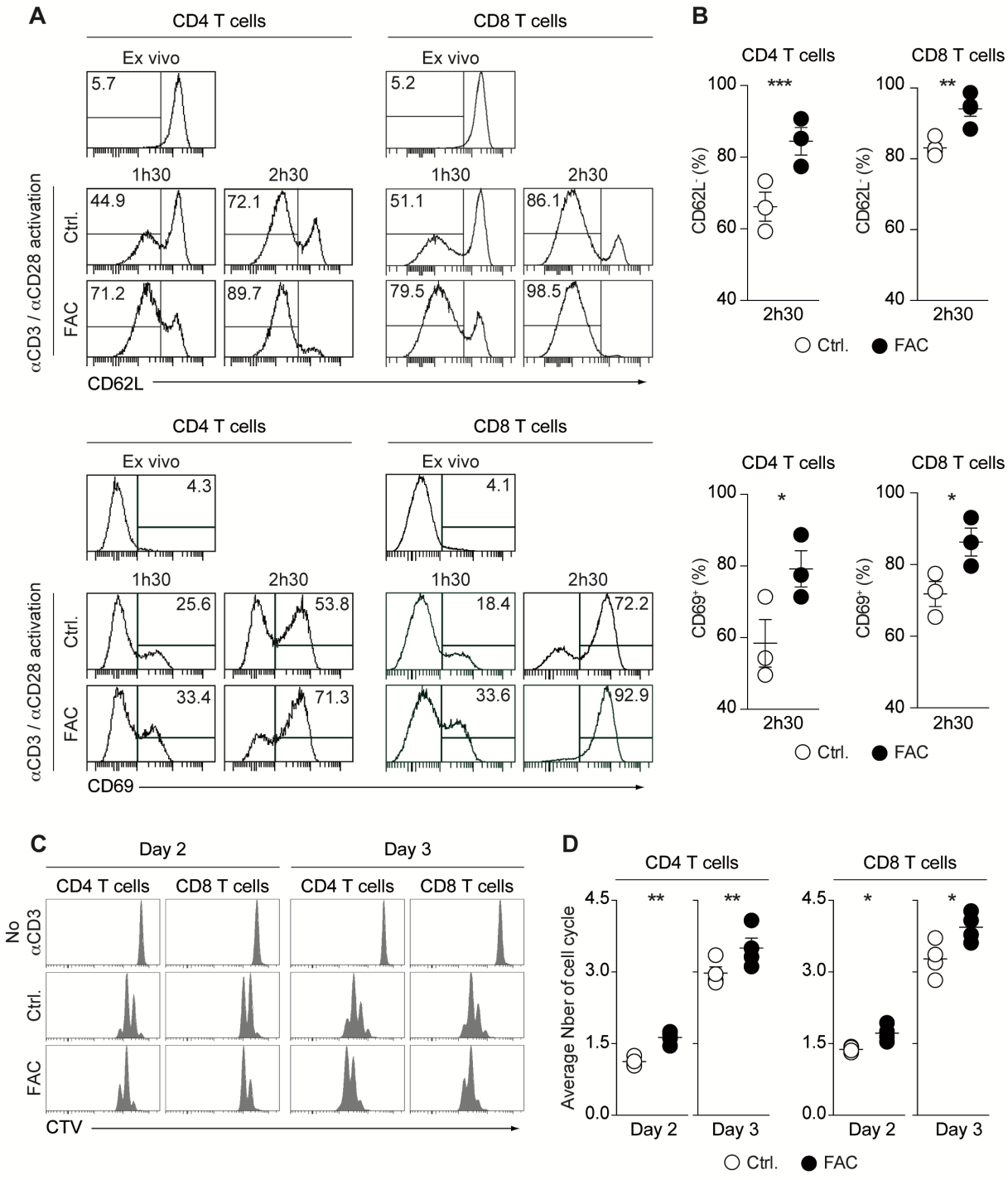
A
CD4 T cells
CD8 T cells
Ex vivo
5.7
5.2
1h30
2h30
αCD3 / αCD28 activation
Ctrl.
FAC
44.9
72.1
51.1
86.1
71.2
89.7
79.5
98.5
CD62L
4.3
4.1
25.6
53.8
18.4
72.2
33.4
71.3
33.6
92.9
CD69
B
CD62L- (%)
CD69+ (%)
***
**
*
Ctrl.
FAC
C
Day 2
Day 3
No αCD3
CTV
D
Average Nber of cell cycle
Day 2
Day 3

**Figure 3**

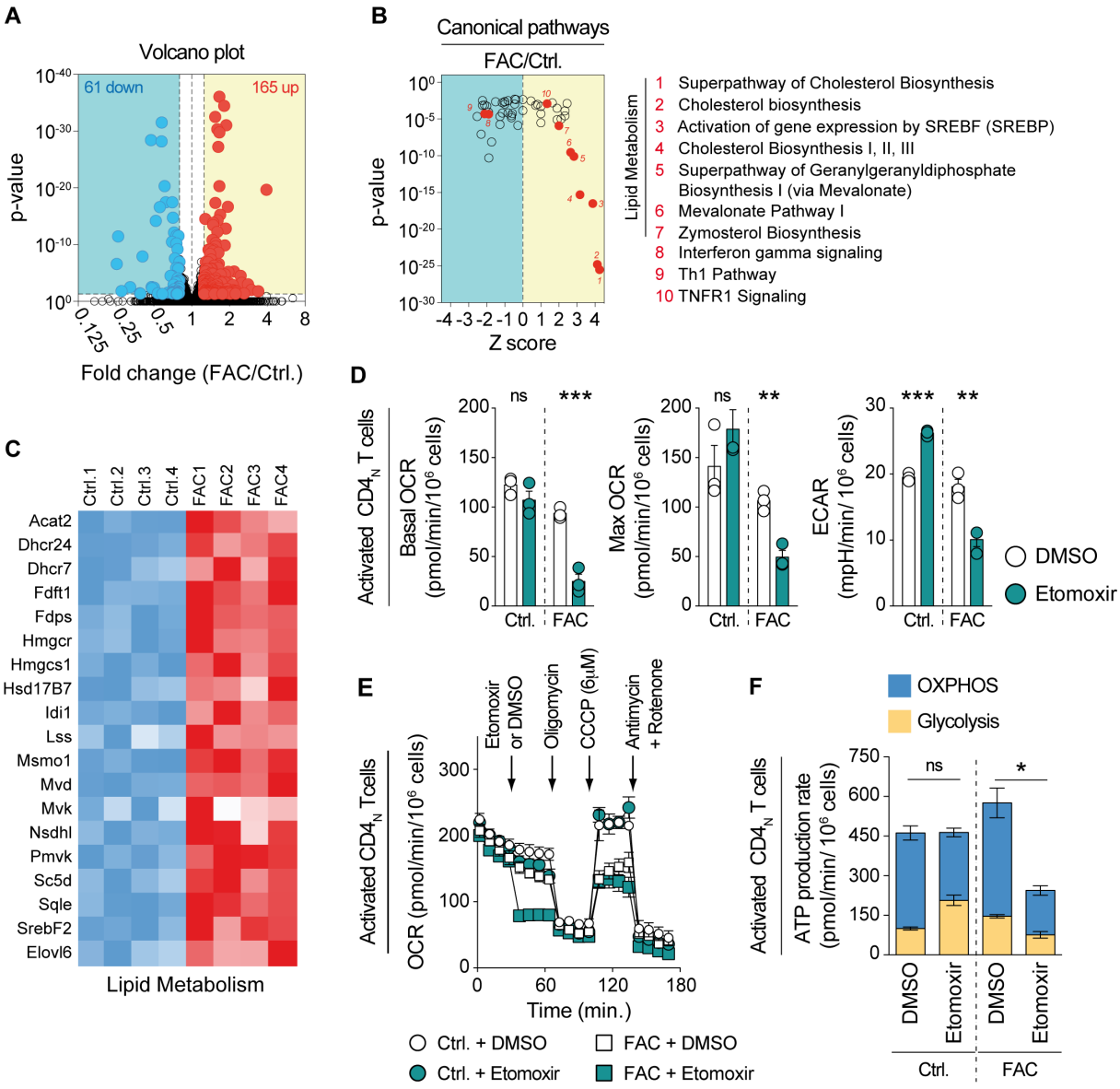
A
Volcano plot
61 down
165 up
p-value
Fold change (FAC/Ctrl.)
B
Canonical pathways
FAC/Ctrl.
p-value
Z score
Lipid Metabolism
1 Superpathway of Cholesterol Biosynthesis
2 Cholesterol biosynthesis
3 Activation of gene expression by SREBF (SREBP)
4 Cholesterol Biosynthesis I, II, III
5 Superpathway of Geranylgeranyldiphosphate Biosynthesis I (via Mevalonate)
6 Mevalonate Pathway I
7 Zymosterol Biosynthesis
8 Interferon gamma signaling
9 Th1 Pathway
10 TNFR1 Signaling
C
Ctrl.1 Ctrl.2 Ctrl.3 Ctrl.4 FAC1 FAC2 FAC3 FAC4
Acat2
Dhcr24
Dhcr7
Fdft1
Fdps
Hmgcr
Hmgcs1
Hsd17B7
Idi1
Lss
Msmo1
Mvd
Mvk
Nsdhl
Pmvk
Sc5d
Sqle
SrebF2
Elovl6
Lipid Metabolism
D
Activated CD4N T cells
Basal OCR (pmol/min/10^6 cells)
Max OCR (pmol/min/10^6 cells)
ECAR (mpH/min/ 10^6 cells)
ns
***
**
Ctrl.
FAC
DMSO
Etomoxir
E
Activated CD4N Tcells
OCR (pmol/min/10^6 cells)
Etomoxir or DMSO
Oligomycin
CCCP (6µM)
Antimycin + Rotenone
Time (min.)
Ctrl. + DMSO
FAC + DMSO
Ctrl. + Etomoxir
FAC + Etomoxir
F
OXPHOS
Glycolysis
Activated CD4N T cells
ATP production rate (pmol/min/ 10^6 cells)
ns
*
DMSO
Etomoxir
Ctrl.
FAC

**Figure 4**

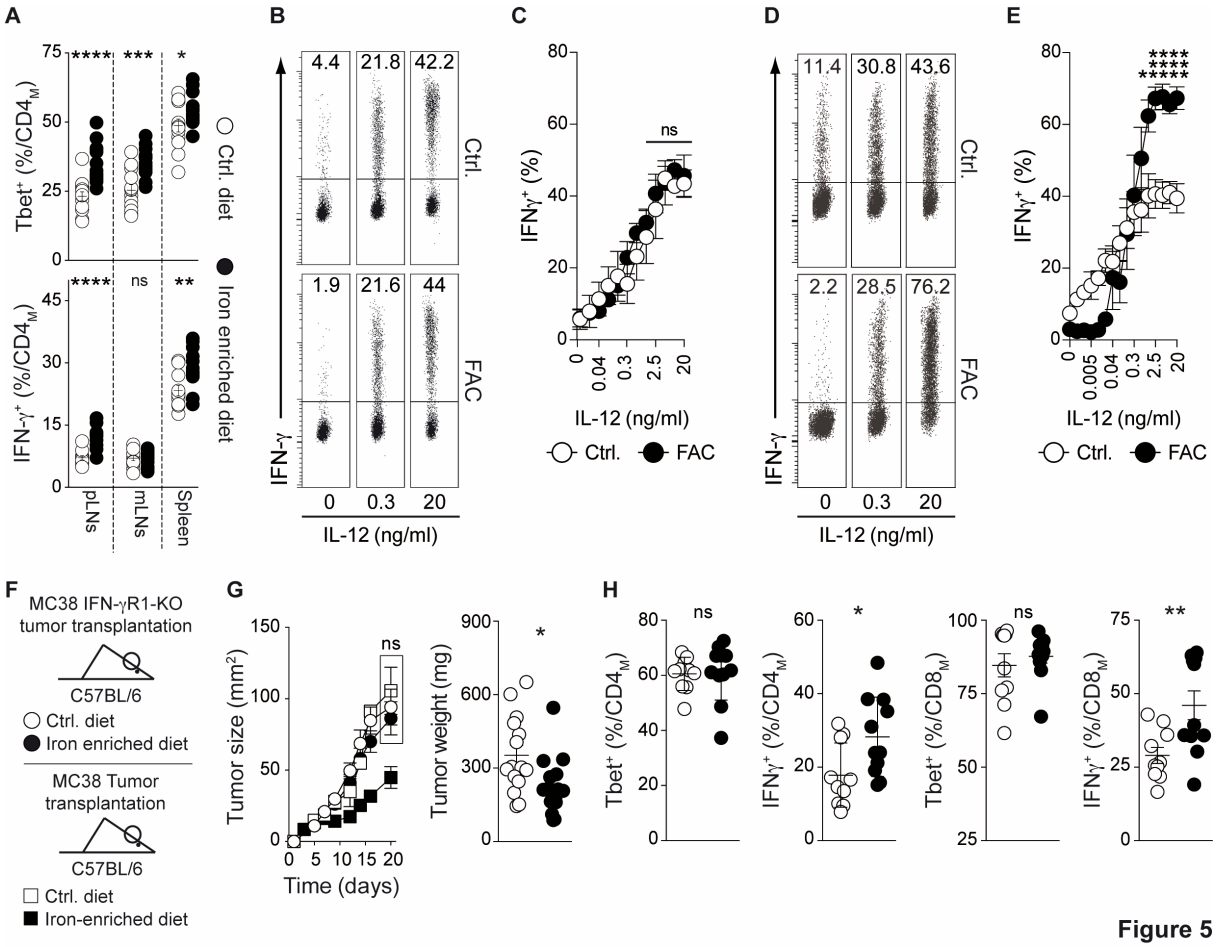
A
B
C
D
E
F
G
H
Ctrl. diet
Iron enriched diet
pLNs
mLNs
Spleen
Ctrl.
FAC
IL-12 (ng/ml)
MC38 IFN-γR1-KO tumor transplantation
C57BL/6
MC38 Tumor transplantation
Ctrl. diet
Iron-enriched diet
Tumor size (mm²)
Time (days)
Tumor weight (mg)

**Figure 5**

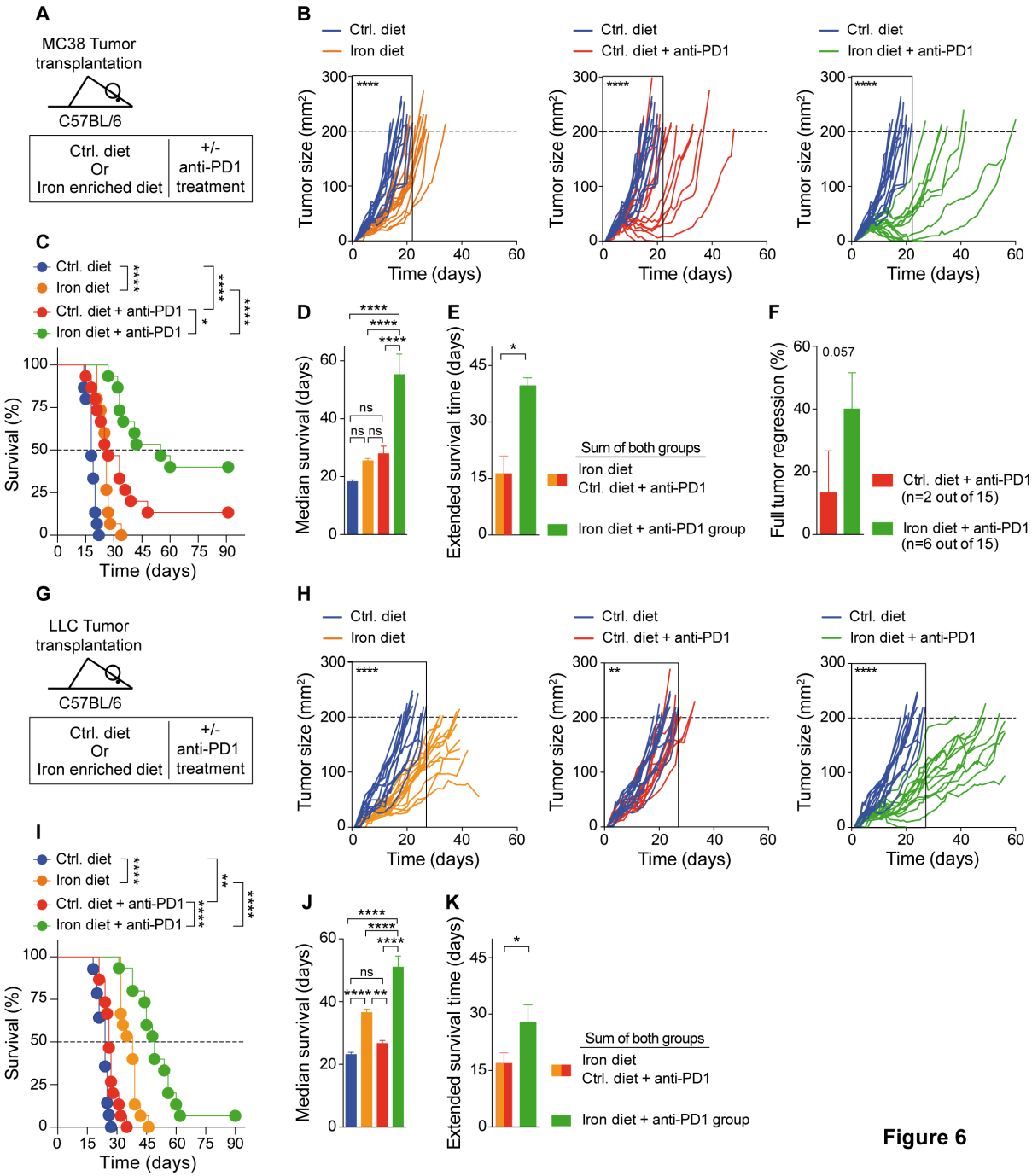
A
MC38 Tumor transplantation
C57BL/6
Ctrl. diet Or Iron enriched diet
+/- anti-PD1 treatment
B
Ctrl. diet
Iron diet
Ctrl. diet + anti-PD1
Iron diet + anti-PD1
Tumor size (mm²)
Time (days)
C
Survival (%)
Time (days)
D
Median survival (days)
ns
E
Extended survival time (days)
Sum of both groups
Iron diet
Ctrl. diet + anti-PD1
Iron diet + anti-PD1 group
F
Full tumor regression (%)
0.057
Ctrl. diet + anti-PD1 (n=2 out of 15)
Iron diet + anti-PD1 (n=6 out of 15)
G
LLC Tumor transplantation
C57BL/6
Ctrl. diet Or Iron enriched diet
+/- anti-PD1 treatment
H
I
J
K

**Figure 6**

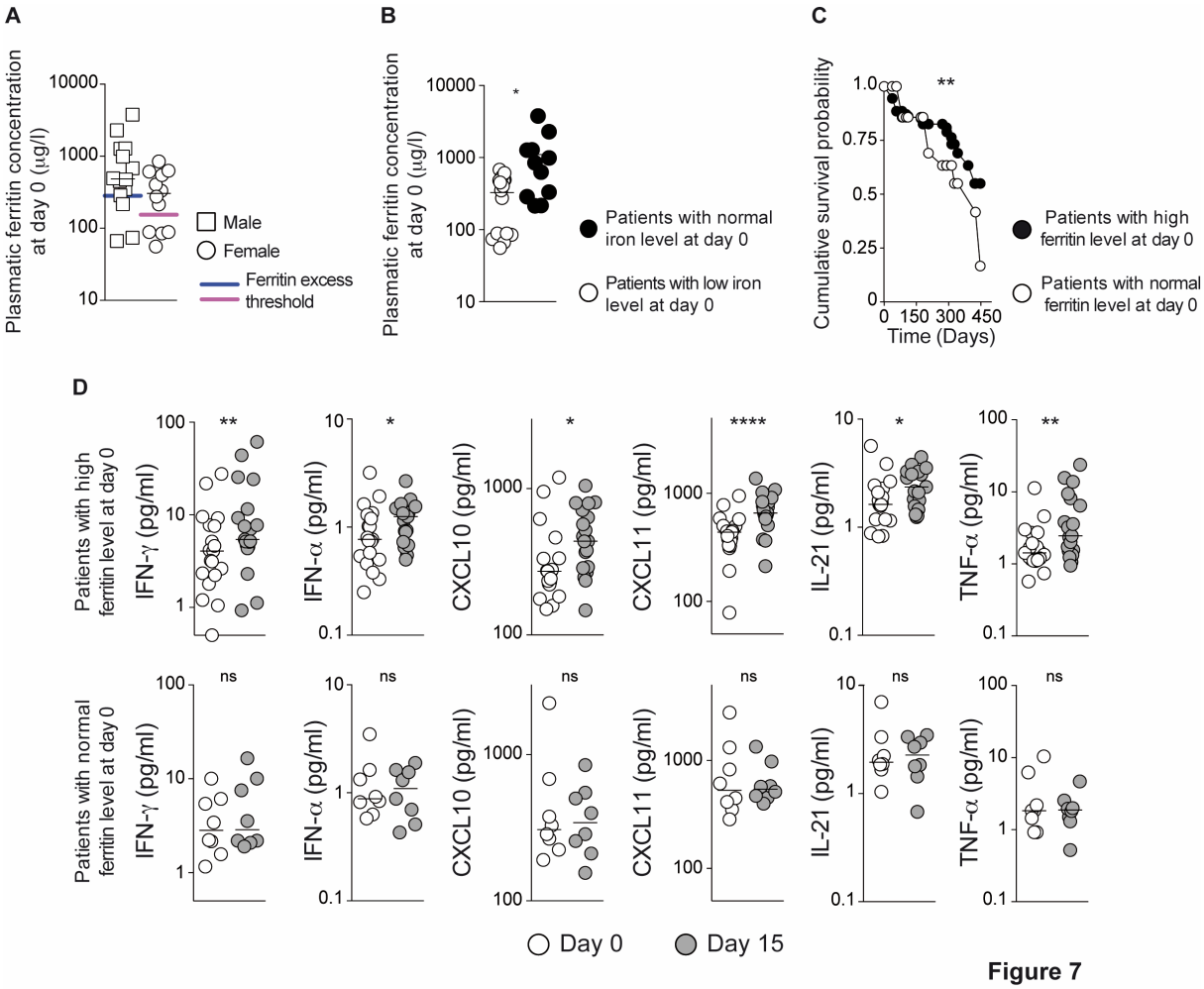
A
Plasmatic ferritin concentration at day 0 (µg/l)
10000
1000
100
10
Male
Female
Ferritin excess threshold
B
Plasmatic ferritin concentration at day 0 (µg/l)
*
Patients with normal iron level at day 0
Patients with low iron level at day 0
C
Cumulative survival probability
1.0
0.75
0.5
0.25
0
**
0 150 300 450
Time (Days)
Patients with high ferritin level at day 0
Patients with normal ferritin level at day 0
D
Patients with high ferritin level at day 0
Patients with normal ferritin level at day 0
IFN-γ (pg/ml)
IFN-α (pg/ml)
CXCL10 (pg/ml)
CXCL11 (pg/ml)
IL-21 (pg/ml)
TNF-α (pg/ml)
**
*
*
****
*
**
ns
Day 0
Day 15

**Figure 7**

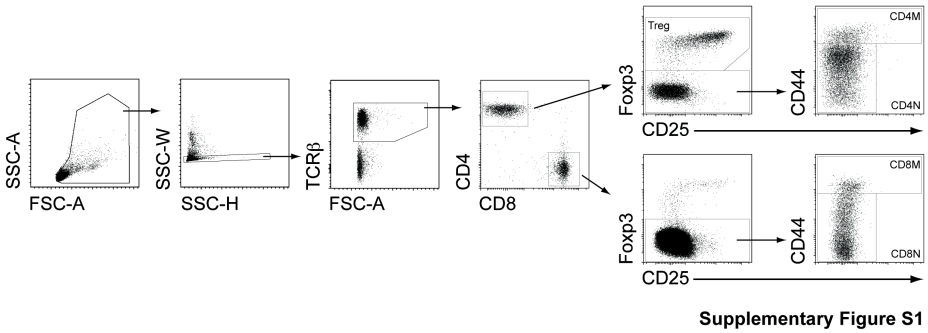


**Supplementary Figure S1**

**Supplementary Figure S1 : Gating strategy defining T-cell subsets**

Gating strategy to define regulatory CD4 T cells (CD4R), effector/memory CD4 T cells (CD4M), naive CD4 T cells (CD4N), effector/memory CD8 T cells (CD8M) and naive CD8 T cells (CD8N).

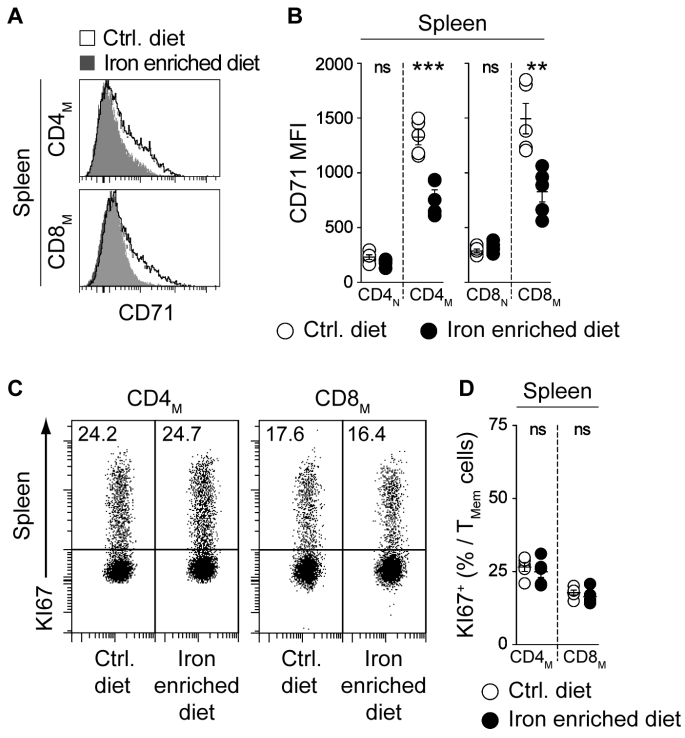


**Supplementary Figure S2**

**Supplementary figure S2: Impact of iron supplementation on CD71 expression by T cells *in vivo***

C57BL/6 mice were fed during 3 weeks with either a control or an iron-enriched diet. (A) Representative CD71 fluorescence histograms of CD4 and CD8 memory T cells recovered from the spleen of mice fed either a control or an iron-enriched diet. (B) CD71 MFI for naïve or memory CD4 and CD8 T cells recovered from the spleen of mice fed either a control or an iron-enriched diet. (C) Representative KI67 dotplots for gated memory CD4 or CD8 T cells recovered from the spleen of mice fed either a control or an iron-enriched diet. (D) Percentages of $KI67^+$ cells among memory CD4 or CD8 T cells recovered from the spleen. Each dot represents individual mice. Data are expressed as mean ± SEM, Student's *t*-test was used (n = 2 independent experiments) (*$p < 0.05$; **$p < 0.01$; ***$p < 0.001$; ****$p < 0,0001$, ns, not significant.).

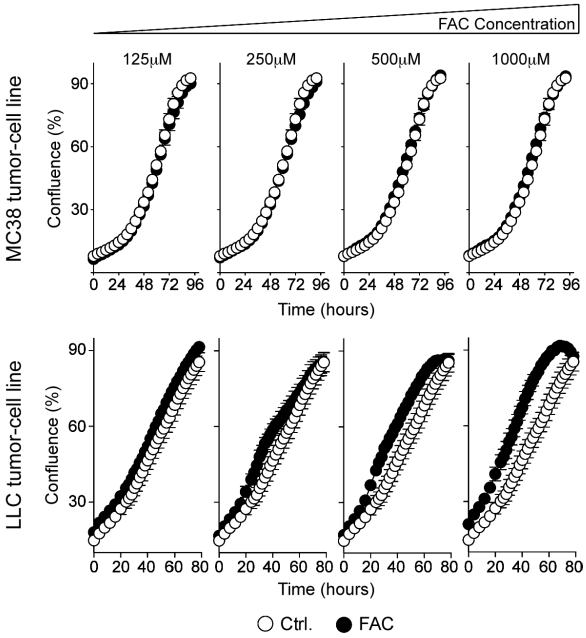


**Supplementary Figure S3**

**Supplementary Figure S3: Iron supplementation does not inhibit MC38 and LLC tumor-cell proliferation *in vitro***

MC38 or LLC tumor cell lines were cultured alone or in the presence of graded doses of FAC. Incucyte technology has been used all along the kinetics to measure the percentage of confluence reflecting cell proliferation. Representative experiment is shown here.

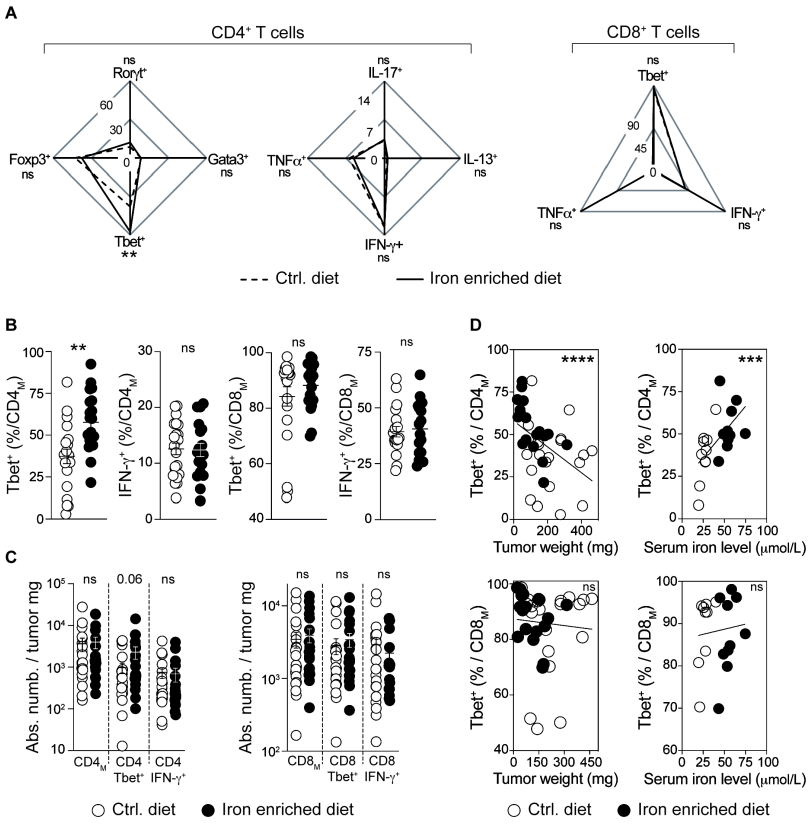


**Supplementary Figure S4**

**Supplementary Figure S4: Iron increases the proportion of Th1 cells in the LLC tumor microenvironment**

$10^6$ LLC tumor cells were transplanted into C57BL/6 mice fed with either a control or an iron-enriched diet. (A) Radar plots illustrating the proportions of the different CD4 and CD8 T-cell subsets among tumor infiltrating T cells. (B) Proportions of Tbet-expressing and IFN-γ producing CD4 or CD8 T cells among tumor infiltrating $CD4_M$ or $CD8_M$ T cells. Each dot represents individual mice. (C) Densities of $CD4_M$, $CD8_M$, Tbet-expressing and IFN-γ producing $CD4_M$ and $CD8_M$ T cells within tumor microenvironments. Each dot represents individual mice. (D) Correlations between either LLC tumor weight at the time of sacrifice or mouse serum iron level with proportions of Tbet expressing-CD4 and CD8 T cells among tumor-infiltrating T cells. For assessing correlations, Pearson correlation (two-sided test, coefficient, and 95% confidence intervals) was used. Data are expressed as mean ± SEM (n = 3 independent experiments). Wilcoxon-Mann's Whitney test was used. (*$p < 0.05$; **$p < 0.01$; ***$p < 0.001$; ****$p < 0{,}0001$, ns, not significant.). Each dot represents individual mice.

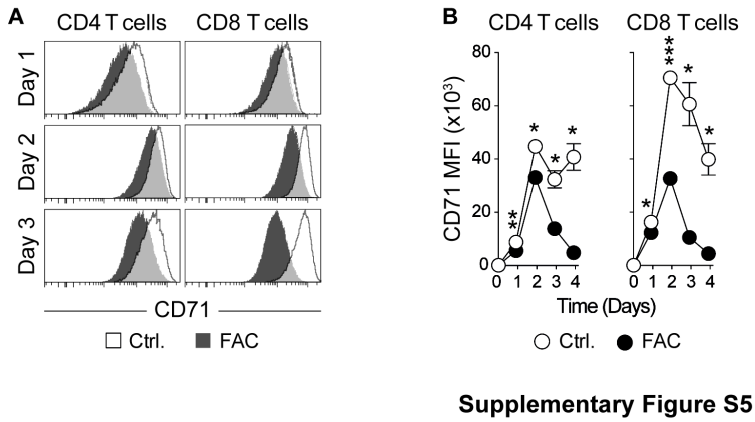


**Supplementary Figure S5**

**Supplementary figure S5: Impact of iron supplementation on CD71 expression by T cells *in vitro***

(A, B) Facs sorted LN naïve CD4 T cells from C57BL/6 were stimulated with coated anti-CD3 and anti-CD28 Abs in the presence or absence of FAC for the indicated time. (C) Representative CD71 fluorescence histograms of stimulated CD4 and CD8 T cells. (D) CD71 MFI of stimulated CD4 and CD8 T cells are shown as a function of time. Data are expressed as mean ± SEM two-tailed paired Student's *t*-test was used (n = 3 independent experiments). (*$p < 0.05$; **$p < 0.01$; ***$p < 0.001$; ****$p < 0,0001$, ns, not significant.).

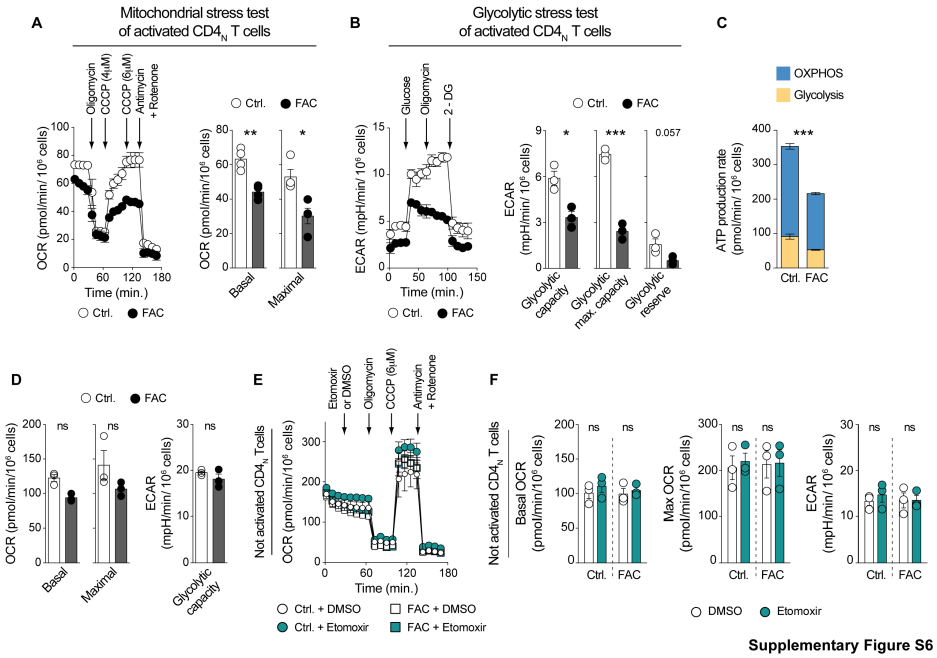


**Supplementary Figure S6: Iron induces T cell metabolic reprogramming**

(A-C) Oxidative and glycolytic capacities were determined using Seahorse in activated $CD4_N$ T, cultured in RPMI (11mM glucose and 2 mM glutamine), in the presence (FAC) or absence (Ctrl.) of iron supplementation. (A) (left panel) Profile after mitochondrial stress assay showing the OCR of activated $CD4_N$ T, in the absence or presence of FAC (n = 3 independent experiments). (Right panel) Graph showing basal and maximal respiration rate (OCR) (n = 3 independent experiments). (B) (left panel) Representative profile after glycolysis stress test showing the ECAR of activated $CD4_N$ T in the absence or presence of FAC (n = 3 independent experiments). (Right panel) Graph showing basal, maximal glycolytic capacities, and glycolytic reserve (n = 3 independent experiments). (C) ATP production rate from glycolysis or oxidative phosphorylation in activated $CD4_N$ T in the absence or presence of FAC (n = 3 independent experiments). (D-F) $CD4_N$ T cells were incubated with 150 mM palmitate/BSA, 5 mM glucose and 2 mM glutamine. (D) Graph showing basal and maximal respiration rate (OCR) and basal glycolytic capacity of activated $CD4_N$ T, in the absence or presence of FAC (n = 3 independent experiments) (E) Profile after mitochondrial stress assay showing the OCR of non-activated $CD4_N$ T, in the absence or presence of FAC (n = 3 independent experiments). (F) Oxidative and glycolytic capacities were determined using Seahorse in non-activated $CD4_N$ T treated with etomoxir (1µM) in the presence (FAC) or absence (Ctrl.) of iron supplementation. Graphs showing basal and maximal respiration rate (OCR), in addition to basal glycolytic capacity (ECAR) (n = 3 independent experiments). Data are expressed as mean ± SEM. Results were assessed using a two-tailed paired Student's *t*-test (*$p < 0.05$; **$p < 0.01$; ***$p < 0.001$; ****$p < 0,0001$, ns, not significant).

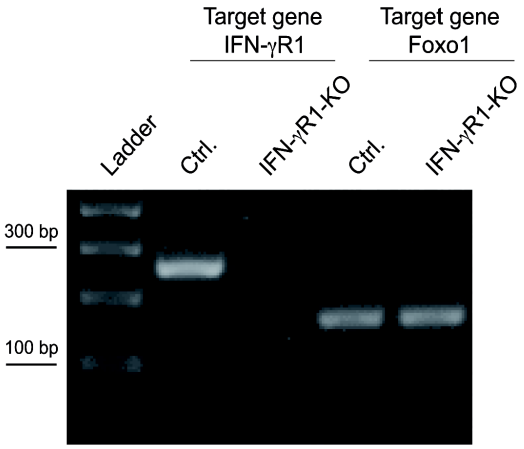


**Supplementary Figure S7**

**Supplementary Figure S7: CRISPR/Cas9 generated MC38 IFN-γR1-KO tumor cell line**

Agarose gel electrophoresis of PCR products from CRISPR/Cas9 generated MC38 IFN-γR1-KO cell line. PCR was done on direct DNA for the MC38 IFN-γR1-KO cell line.

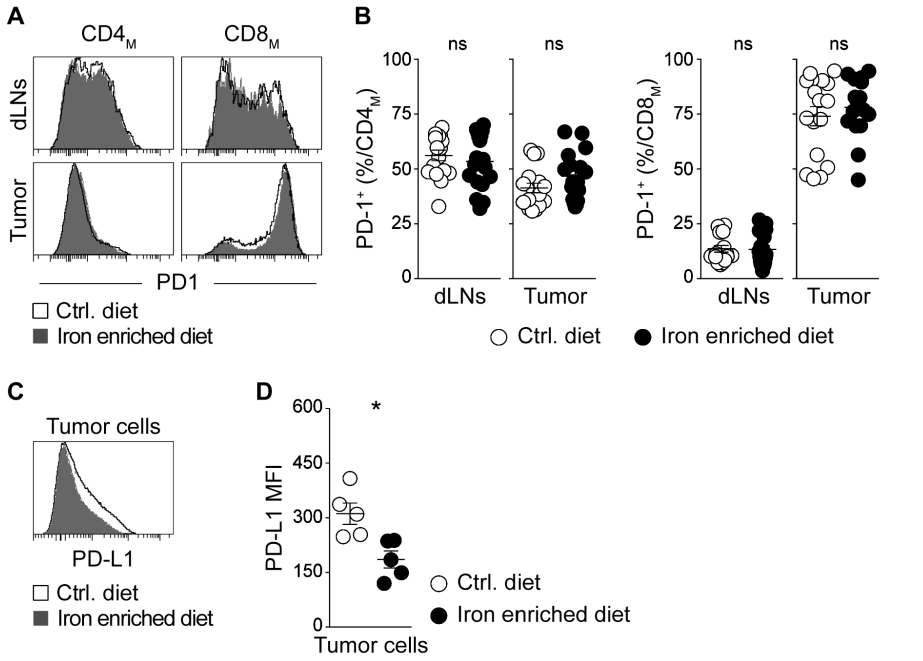


**Supplementary Figure S8**

**Supplementary Figure S8: Impact of iron on the expression of PD1 or PD-L1 on T cells or tumor cells respectively**

$10^6$ MC38 tumor cells were transplanted into C57BL/6 mice fed with either a control or an iron-enriched diet. (A) Representative PD1 fluorescence histograms of CD4 and CD8 memory T cells recovered from tumor draining LNs (dLNs) or tumor of mice fed either a control or an iron-enriched diet, 14 days after tumor cell transplantation. (B) Proportions of PD1-expressing CD4 or CD8 T cells among $CD4_M$ or $CD8_M$ T cells recovered from dLNs or tumor of mice fed either a control or an iron-enriched diet, 14 days after tumor cell transplantation. (n = 3 independent experiments). Each dot represents individual mice. (C) Representative PD-L1 fluorescence histograms of MC38 tumor cells recovered from mice fed either a control or an iron-enriched diet, 14 days after tumor cell transplantation. (D) PD-L1 MFI of MC38 tumor cells recovered from mice fed either a control or an iron-enriched diet, 14 days after tumor cell transplantation. Each dot represents individual mice. Data are expressed as mean ± SEM. (n = 2 independent experiments). Wilcoxon-Mann's Whitney test was used. (*$p < 0.05$; **$p < 0.01$; ***$p < 0.001$; ****$p < 0,0001$, ns, not significant.).

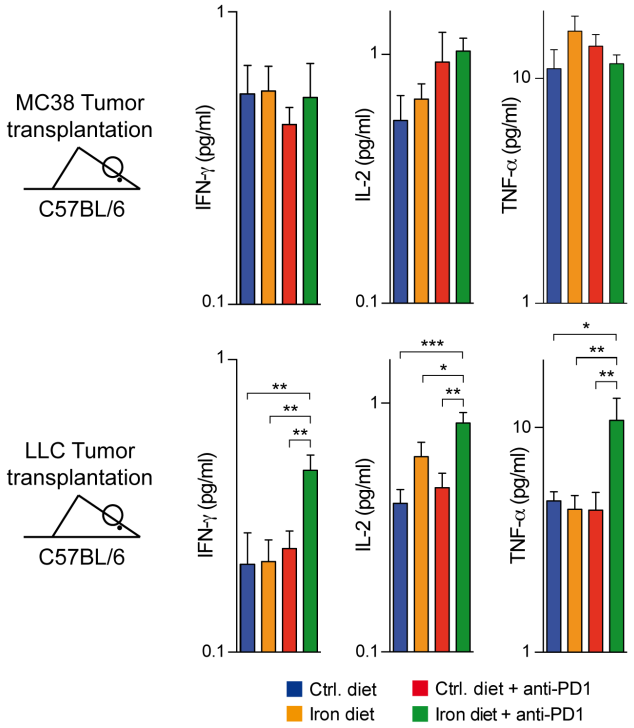


**Supplementary Figure S9**

**Supplementary Figure S9: Iron and anti-PD1 cancer immunotherapy combination increases serum concentrations of IFN-γ, TNF-α and IL-2 in LLC tumor transplanted mice**

$10^6$ MC38 or LLC tumor cells were transplanted into C57BL/6 mice fed with either a control or an iron-enriched diet. For concerned groups, anti-PD1 immunotherapy was administered once tumor size reached 20-25mm$^2$. Serum concentrations of IFN-γ, IL-2 and TNF-α for the different groups of MC38 or LLC tumor bearing mice. (n = 3 independent experiments). Data are expressed as mean ± SEM. Wilcoxon-Mann's Whitney test was used. (*$p < 0.05$; **$p < 0.01$; ***$p < 0.001$; ****$p < 0{,}0001$, ns, not significant).

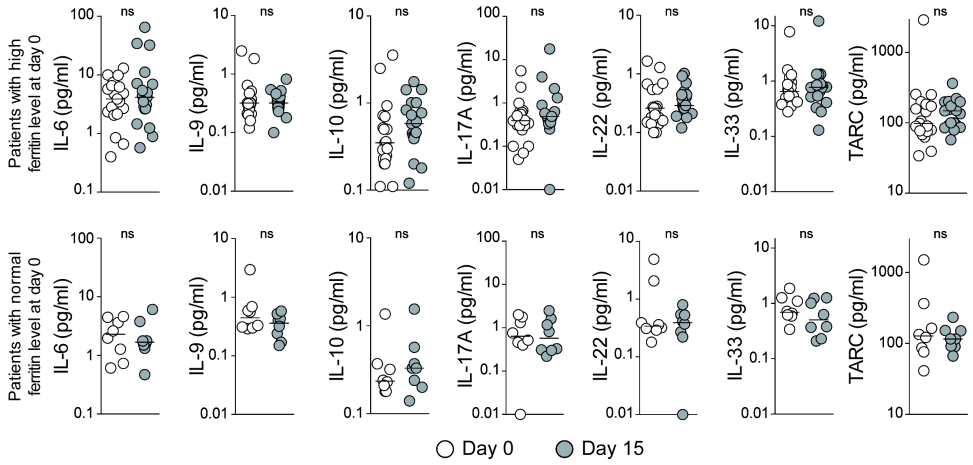


**Supplementary Figure S10**

**Supplementary Figure S10: Body ferritin level does not modulate plasma concentrations of IL-6, IL-9, IL-10, IL-17A, IL-22, IL-33 or TNFα following anti-PD1 immunotherapy in cancer patients**

Plasmatic concentrations of IL-6, IL-9, IL-10, IL-17A, IL-22, IL-33 and TARC at day 0 and day 15 (after nivolumab cure) from patients with high or normal plasmatic ferritin level at day 0. Each dot represents individual patients. Data are expressed as median. Wilcoxon-Mann's Whitney test was used. (*$p < 0.05$; **$p < 0.01$; ***$p < 0.001$; ****$p <$ 0,0001, ns, not significant).

**Supplementary Table S1 : List of used antibodies**

| Antibody | Fluorochrome | Vendor/Company | Catalogue Number | RRID |
|---|---|---|---|---|
| Anti-mouse CD4 | BV510 | Biolegend | 100559 | AB_2562608 |
| Anti-mouse CD4 | PerCP-Cy5.5 | BD Biosciences | 550954 | AB_393977 |
| Anti-mouse CD8a | APC-Vio770 | Miltenyi Biotec | 130-102-305 | AB_2659897 |
| Anti-mouse CD8b2 | PE | BD Biosciences | 553041 | AB_394577 |
| Anti-mouse/human CD11b | PE | BD Biosciences | 553311 | AB_394775 |
| Anti-mouse CD11c | PE | BD Biosciences | 553802 | AB_395061 |
| Anti-mouse CD19 | PE | BD Biosciences | 557399 | AB_396682 |
| Anti-mouse CD25 | PE | BD Biosciences | 553866 | AB_395101 |
| Anti-mouse CD25 | BV650 | Biolegend | 102038 | AB_2563060 |
| Anti-mouse CD44 | PE-Cy7 | BD Biosciences | 560569 | AB_17274843 |
| Anti-mouse/human CD44 | BV785 | Biolegend | 103059 | AB_2571953 |
| Anti-mouse CD45 | BUV395 | BD Biosciences | 564279 | AB_2651134 |
| Anti-mouse CD45 | PE-Cy7 | BD Biosciences | 552848 | AB_394489 |
| Anti-mouse CD45 | BV711 | Biolegend | 103147 | AB_2564383 |
| Anti-mouse CD45 | PerCP-Cy5.5 | BD Biosciences | 550994 | AB_394003 |
| Anti-mouse CD62L | BV650 | BD Biosciences | 564108 | AB_2738597 |
| Anti-mouse CD69 | PE | BD Biosciences | 553237 | AB_394726 |
| Anti-mouse CD71 | PE | Biolegend | 113807 | AB_313568 |
| Anti-mouse PD1 | PE-Cy7 | Biolegend | 135216 | AB_10689635 |
| Anti-mouse PD-L1 | BV650 | Biolegend | 124336 | AB_2734192 |
| Anti-mouse/Rat Foxp3 | Fitc | eBioscience | 11-5773-82 | AB_465243 |
| Anti-mouse NK1.1 | PE | BD Biosciences | 553165 | AB_394677 |
| Anti-mouse TCRβ | PerCP-Cy5.5 | eBioscience | 45-5961-82 | AB_925763 |
| Anti-mouse TCRβ | Alexa Fluor 700 | BioLegend | 109224 | AB_1027648 |
| Anti-mouse TCRγδ | PE | BD Biosciences | 553178 | AB_394689 |
| Anti-mouse IL-17A | V450 | BD Biosciences | 560522 | AB_1727540 |
| Anti-mouse IL-13 | PECy7 | eBioscience | 25-7133-82 | AB_2573530 |
| Anti-mouse IFN-γ | PE | BD Biosciences | 554412 | AB_395376 |
| Anti-mouse TNF-α | APC | BD Biosciences | 554420 | AB_398553 |
| Anti-mouse T-bet | PEVio615 | Miltenyi | 130-121-998 | AB_2784466 |
| Anti-mouse GATA3 | BV711 | BD Biosciences | 565449 | AB_2739242 |
| Anti-mouse/human RORγt | APC | Miltenyi | 130-103-838 | AB_2653366 |
| Anti-mouse Ki67 | Alexa Fluor 647 | Biolegend | 151206 | AB_2566801 |
| Anti-mouse CD3ε | | from hybridoma supernatant (145-2C11) our lab | | |
| Anti mouse-CD8a | | from hydridoma supernatant (53-6.7) our lab | | |
| Anti-mouse CD11b | | from hydridoma supernatant (MAC1) our lab | | |
| Anti-mouse CD19 (1D3) | | BioXcell | BE0150 | AB_10949187 |
| Anti-mouse CD28 purified ultra LEAF | | Biolegend | 102122 | AB_2810331 |
| Anti-mouse Ter-119 (TER-119) | | BioLegend | 116255 | AB_2832401 |
| Anti-mouse PD1 purified ultra-LEAF (clone RMP1-14) | | Biolegend | 114122 | AB_2800578 |

**Supplementary Table S2**

| **Baseline characteristics** | Patient with normal ferritin level at day 0 | Patient with High ferritin level at day 0 | p |
|---|---|---|---|
| Nb of patients (tot=27) | n = 8 (29.6%) | n = 19 (70.4%) | |
| **Epidemiological features** | | | |
| Age at diagnosis, y, mean ± SEM | 69.6 ± 2.3 | 64.5 ± 2.1 | 0.1570 |
| Male, n (%) | 4 / 8 (50) | 11 / 19 (58) | |
| Female, n (%) | 4 / 8 (50) | 8 / 19 (42) | |
| **Biologic features** | | | |
| C-reactive protein (CRP) mg/L, mean ± SEM | 11.2 ± 3.3 | 28.2 ± 8.5 | 0.2073 |
| Albumin g/L, mean ± SEM | 40.4 ± 0.9 | 39.3 ± 1.4 | 0.6182 |
| Orosomucoid g/L, mean ± SEM | 1.1 ± 0.2 | 1.4 ± 0.1 | 0.1884 |
| IgG g/L, mean ± SEM | 9.5 ± 1.1 | 11.8 ± 0.8 | 0.1201 |

**Supplementary Table S2 : Epidemiological features of studied patients with lung cancer**

Cohort of patients was dichotomized according to plasma ferritin levels. Data are expressed as mean ± SEM Wilcoxon-Mann's Whitney test was used. (*$p < 0.05$; **$p < 0.01$; ***$p < 0.001$; ****$p < 0,0001$, ns, not significant).